ANALYSIS OF WATER FLOWBACK DATA IN GAS SHALE RESERVOIRS

A Thesis

by

HUSSAIN YOUSEF H. ALDAIF

Submitted to the Office of Graduate and Professional Studies of
Texas A&M University
in partial fulfillment of the requirements for the degree of

MASTER OF SCIENCE

Chair of Committee,	David S. Schechter
Committee members,	Hadi Nasrabadi
	Marcelo Sanchez
Head of Department,	A. Daniel Hill

December 2014

Major Subject: Petroleum Engineering

ABSTRACT

Properties of both shale gas reservoirs and hydraulic fractures are usually estimated by analyzing hydrocarbon production data while water data is typically ignored. This study introduces a new method to estimate the effective fracture volume in shale gas wells using water production data instead of the hydrocarbon production data.

The main objective of this study is to verify and improve Alkouh's method of estimating the effective fracture volume using water production data through testing it at different reservoir conditions. For this purpose, several simulation cases were run. The results of the simulation runs were compared with the production data from several Fayetteville gas wells. Different conclusions were obtained from these comparisons that emphasize the importance of using water production data in the production data analysis. A better evaluation for fracture-stimulation jobs can be acquired through the estimation of the effective fracture volume from early water production data.

The main outcome of this study is a new method (modification of Alkouh's method) for analyzing water production data in shale gas wells. The new method gave very good estimation to the actual effective fracture volume in all simulation cases while Alkouh's method overestimated the volume in all cases. In addition, the new method considered the effect of changing initial reservoir pressure (different reservoirs) and flowing bottom-hole pressure. In addition, the new method showed very good estimation of the effective fracture volume when applied on field data. The data of the first 10-15 days of production (early production data) was used to evaluate the fracture job using the

new method and it only underestimated the actual volume (after few years of water production) by around 10%.

DEDICATION

I dedicate my work for my parents, Yousef and Amal, for my wife, Zahra, for my brothers, Hassan and Mohammed, and for my sisters, Fatima, Zainab and Zahra.

ACKNOWLEDGEMENTS

First, I would like to give praises and honor to Allah almighty for his infinite mercies and blessings.

I would like to thank my father and my mother for their prayers and support. In addition, I would like to thank my wife for her patience, prayers, love and support without which this work would not be accomplished.

I would like to thank Dr. Abdul Aziz Dejain for nominating me to pursue my master degree in petroleum engineering.

I would like to thank Saudi Aramco management for the scholarship to purse my graduate studies.

I would like to express my appreciation to my previous research advisor and committee chair, Dr. Robert A. Wattenbarger, for his valued guidance and inspiration. It has been an honor working with him for around fifteen months. In addition, I would like to thank my current advisor and committee chair, Dr. David S. Schechter, for his help and support. I would like to thank Dr. Hadi Nasrabadi and Dr. Marcelo Sanchez for serving on my advisory committee. I would like to thank Dr. Pope for his acceptance to attend my defense and for his valuable comments that improved the quality of my thesis.

I would like to thank my Aggie friends; Zuhair Al Yousef, Murtada AlJawad, Hussain AlBahrani, Mohanned Bukhamseen, Hamed Alhoori and Mohammed AlSamahiji for their support and friendship.

Finally, I would like to thank my colleagues; Ahmad Alkouh, Basil Alotaibi, Mohammed Kanfar, Pahal Sinurat and Mohit Dohli for their help and support which improved the quality of this work.

NOMENCLATURE

B_w	Water formation volume factor, res Bbl/STB
c_g	Gas compressibility, psi^{-1}
c_f	Formation compressibility, psi^{-1}
c_t	Total compressibility, psi^{-1}
c_w	Water compressibility, psi^{-1}
h	Reservoir thickness, ft
k_{rg}	Relative permeability to gas, fraction
k_{rw}	Relative permeability to water, fraction
k_m	Matrix permeability, md
L_F	Fracture spacing, ft
p_i	Initial reservoir pressure, psi
p_{wf}	Flowing bottom-hole pressure, psi
q_g	Gas flow rate, Mscf/D
T	Temperature, ^oF
V_w	Water volume, STB
x_f	Fracture half length, ft

Abbreviations

BDF	Boundary dominated flow
MEFV	Minimum effective fracture volume
MFHW	Multi-fractured horizontal wells

PSS	Pseudo-steady state
RNP	Rate normalized pressure, psi/STB/D

Greek Symbols

ϕ	Porosity, fraction
γ	Gas specific gravity, fraction

Subscripts

i	Initial Condition
f	Formation
F	Hydraulic fracture
g	Gas
m	Matrix
t	Total system
w	Water

TABLE OF CONTENTS

Page

LIST OF FIGURES

Page

LIST OF TABLES

Page

CHAPTER I

INTRODUCTION

The gas and oil industry has been investing in shale plays for the last few years. Drilling multi-fractured horizontal wells (MFHW) is the technique that made producing those unconventional resources economical and profitable. Drilling MFHW requires using large amounts of slickwater in order to create a hydraulic fracture network in each well.

Typically, reservoir engineers use the gas/oil production data in order to both analyze the well performance and determine the fracture properties. Based on the production data, the engineer can evaluate the fracturing job and decide whether the well needs to be re-completed or not.

Several authors have argued that water flowback data should not be ignored and can be useful in characterizing the fracture network (Abbasi et al. 2012, Alkouh et al, 2013, Clarkson 2012). More details about the uses of water flowback data will be discussed in the literature review chapter.

In this research, data from Fayetteville reservoir were used to investigate the possibility of analyzing water flowback data in shale gas wells.

1.1 Objective

Ahmad Alkouh, in his PhD dissertation, introduced a method to estimate the fracture effective volume in shale gas wells using water flowback data. One of his

objectives was to be able to effectively evaluate fracturing job using water flowback data in gas wells.

The main objective of this my work is to evaluate Ahmad's work and improve it in order to have a better estimation of the fracture effective volume in shale gas reservoirs.

1.2 Thesis Organization

This thesis is divided into five chapters. The organization of these chapters is as follows:

Chapter I include a brief introduction to the subject of this research and the research objective.

Chapter II is a literature review discussing the history of dual porosity models, the flow regimes in shale reservoirs, and most importantly the usage of water production data in analyzing shale wells.

Chapter III explains the method developed by Alkouh in his PhD dissertation and illustrates its issues. A new method is introduced in this chapter in order to improve Alkouh's method.

Chapter IV shows several field examples to test the method introduced in the previous chapter.

Chapter V presents the conclusions obtained from this research.

CHAPTER II

LITERATURE REVIEW

In this chapter, different aspects related to shale reservoirs will be discussed. First, a brief description of the dual porosity system will be presented. Then, we will discuss the different flow regimes in shale and their applications in reservoir and fracture characterization. Finally, a review of papers that analysis water flowback data will be presented.

2.1 Dual Porosity Model

Dual porosity model was introduced in order to describe naturally fractured reservoirs. In the dual porosity system, reservoir matrix represents the primary porosity of the system and has low contribution to the flow capacity. The fracture network, in the other hand, controls the flow capacity and has a negligible storage capacity.

A sugar cube dual porosity model was proposed by Warrant and Root (1963), Fig. 1. In this model, flow between matrix and fracture was assumed to be in pseudo-steady state (PSS).

Kazemi (1969) proposed another dual porosity model where the flow between matrix and fracture was transient, which is the case in shale wells. In this model, the matrix was logarithmically gridded with thin horizontal fractures (slab case), Fig. 2. The difference between Warren and Root model and Kazemi model occur in the transition period between fracture and matrix system as shown in Fig. 3.

De Swaan (1976) derived the analytical solution for radial infinite acting fractured reservoirs. His solution showed a good agreement with numerical results (Kazemi (1969)). However, De Swaan did not have an analytical description for the transition period between the two straight lines shown in Fig. 4.

Serra et al. (1983) used an identical model to that of De Swaan and they divided the production data into three flow regimes; flow regime 1 (early time), flow regime 2 (transition period) and flow regime 3 (late time). Flow regimes 1 and 3 are similar to Warren and Root early and late time. The main addition in their work is that they introduced a solution for flow regime 2 which is a semi-log straight line with a slope equals to one half of the slope of flow regimes 1 and 3.

Chen et al. (1985) extended Serra's work by introducing flow regime 4 and 5 for bounded reservoirs. In their model, flow regime 3 and 4 represent the flow between the matrix and fracture and cannot co-exist. Regime 5 occurs if both matrix and fracture flow are in PSS.

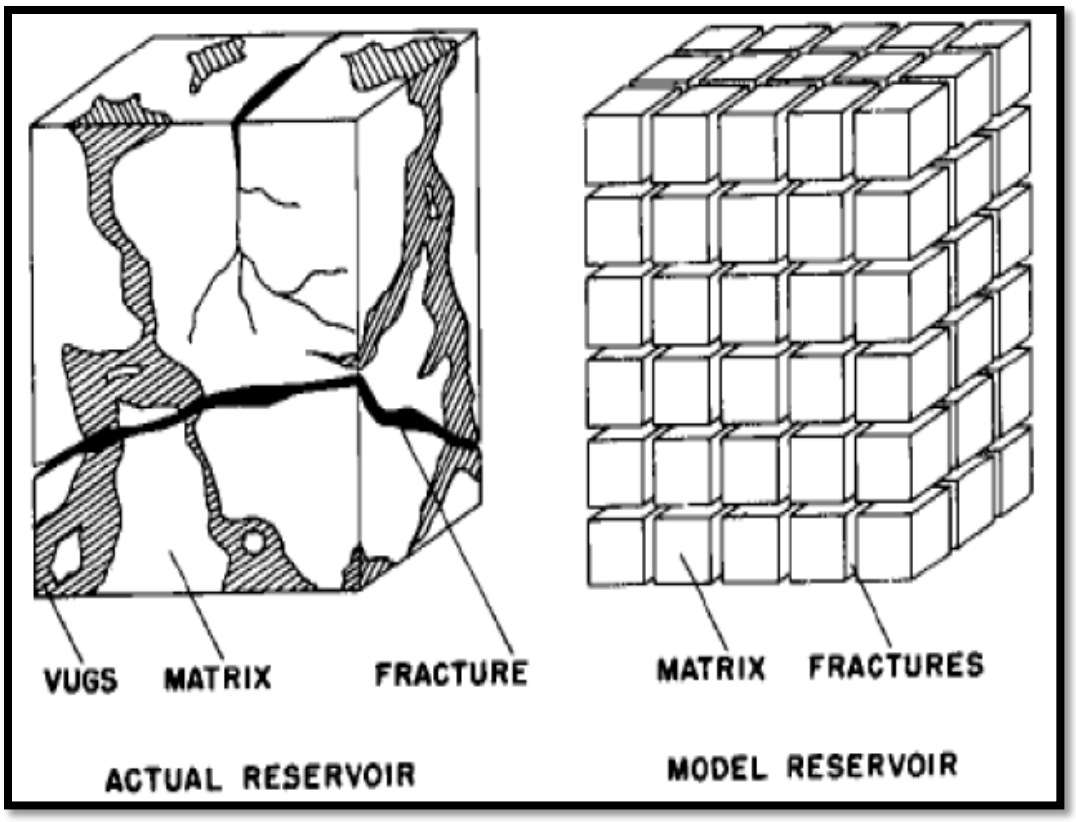

Fig. 1. Warren and Root dual porosity model. (Warren and Root 1963)

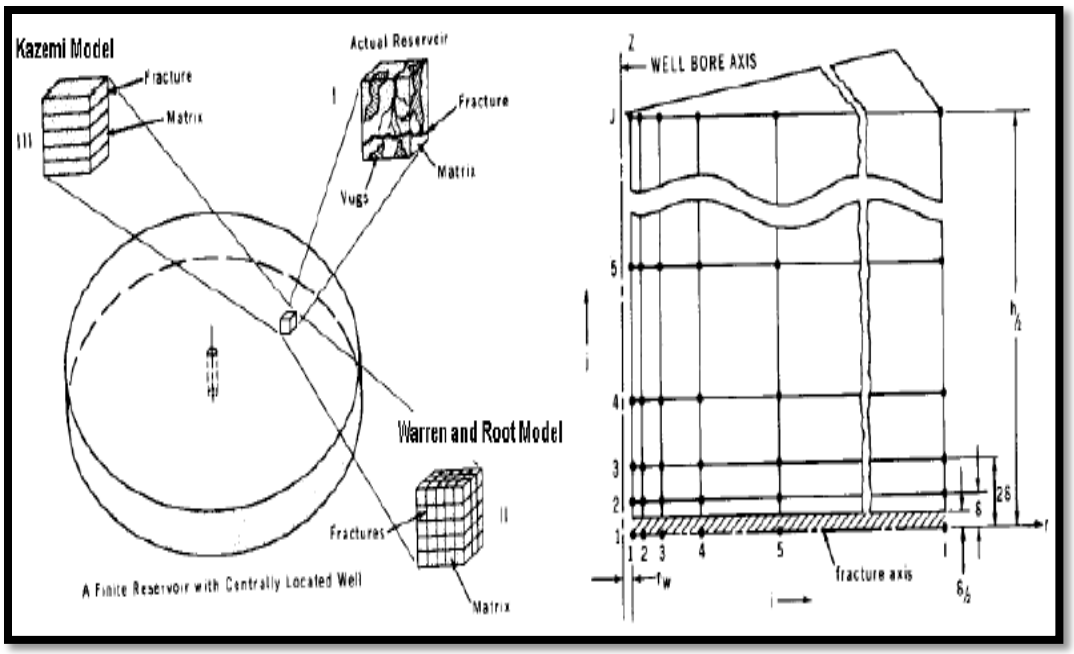

Fig. 2. Kazemi dual porosity model. (Kazemi 1969)

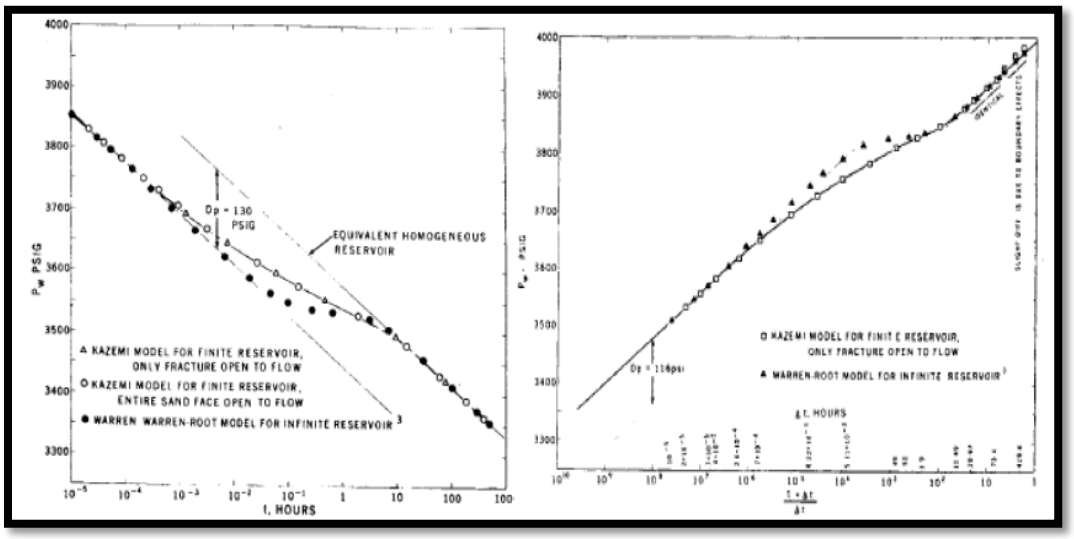

Fig. 3. Comparison between Warren and Root and Kazemi results (Kazemi 1969). The results of the model introduced by Kazemi matches Warren and Root results in the early and late time. The difference occur in the trasition period between fracture and matrix system (transient flow).

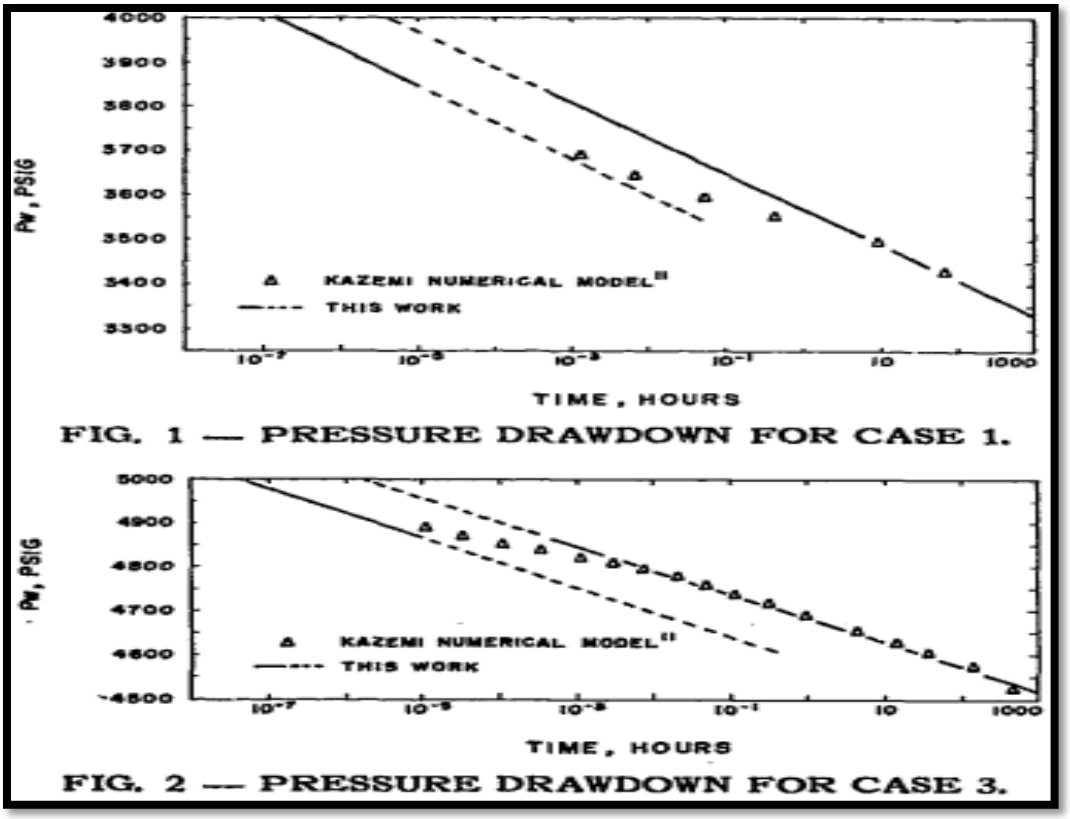

Fig. 4. Comparison between De Swaan and Kazemi results. (De Swaan 1976)

The models discussed earlier were used to describe radial reservoir systems. El-Banbi and Wattenbarger (1998) introduced the solution for dual porosity model with linear flow. In tight/shale reservoirs with multiple fractures, linear flow will dominate the flow and can last for several years as shown in Fig.5 and Fig. 6. Other flow regimes that may exist in shale are bilinear flow and boundary dominated flow (BDF).

2.2 Flow Regimes in Shale

There are three main flow regimes in fractured shale reservoirs. Bilinear flow is the first flow to occur where there is a linear flow from the matrix to the fracture network coinciding with another linear flow from the fracture network to the wellbore. This flow, if it ever occurs, lasts for a very short period of time (hours or days). This flow shows a ¼ slope in both log-log plot (time vs. gas rate in Mscf/D) and the material balance plot.

Bilinear flow is followed by a linear flow from the matrix to the fracture network. This is the dominant flow regime and it shows a ½ slope in both log-log plot and material balance plot.

Finally, BDF will occur once the reservoir boundary is observed. BDF shows an exponential decline in log-log plot while it shows a unit slope in the material balance plot. Those flow regimes are illustrated in both Fig.5 and Fig. 6.

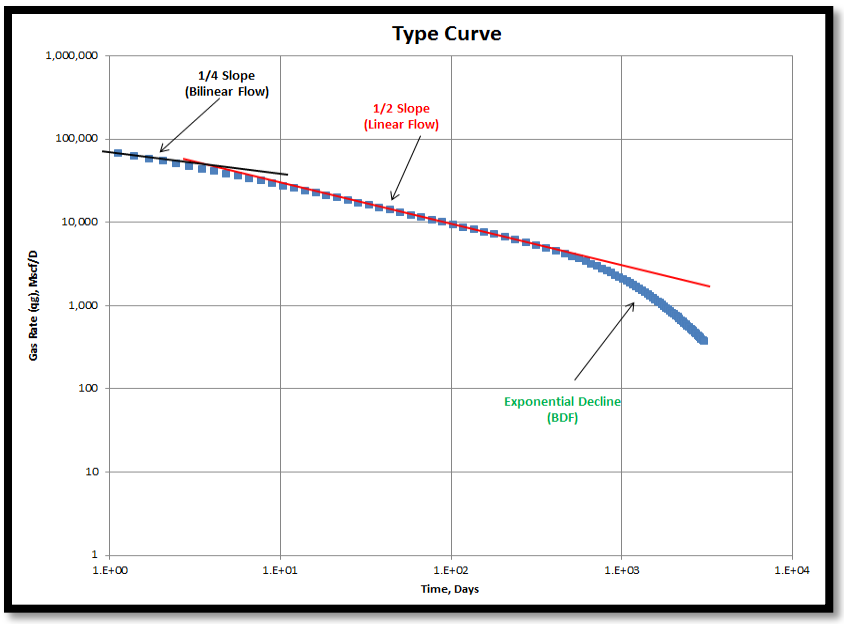

Fig.5. Flow regimes in fractured shale reservoir in a log-log rate vs. time plot.

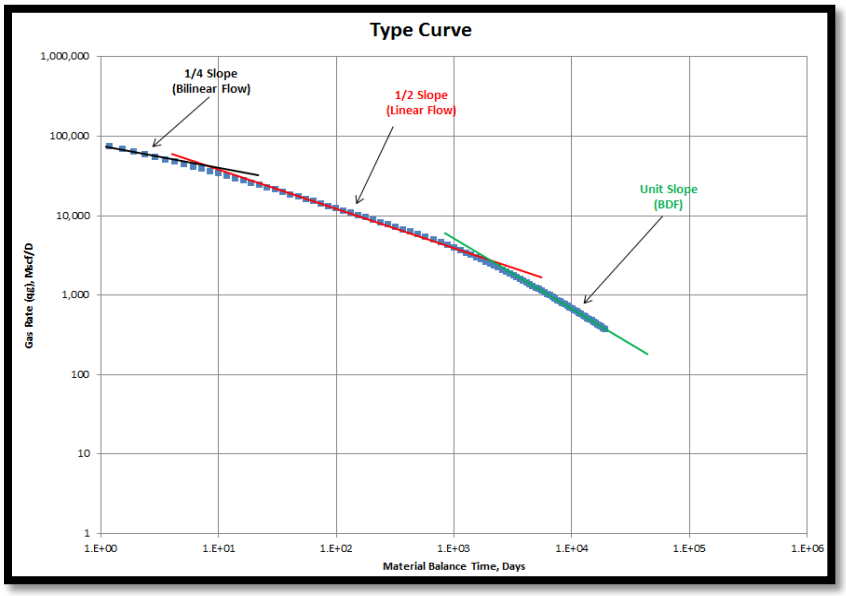

Fig. 6. Flow regimes in fractured shale reservoir in a log-log rate vs. material balance time plot.

2.3 Analysis of Water Flowback Data

Very few authors have discussed the use of water flowback data in estimating fracture properties or evaluating fracture volume. This might be because reservoir engineers will typically analyze the oil/gas data and will ignore the water production data Alkouh et al. (2013).

Abbasi et al. (2012) proposed a method for fracture characterization using water flowback data. In their work, they divided the flowback data into three different regions; region 1, region 2 and region 3. In region 1, water dominates the flow and it is the best period to be analyzed since it satisfies their assumption of having single phase fluid. In the region 2, the oil/gas rate starts to increase until it dominates the flow in the region 3. The authors use rate normalized pressure (RNP) and material balance time to determine hydraulic fracture properties such as fracture permeability and fracture geometry.

Clarkson (2012), Clarkson and Williams-Kovacs (2013), and Williams-Kovacs and Clarkson (2013) have proposed methods to estimate fracture permeability and fracture half-length in both gas (two phase) and oil (three phase) shale reservoirs using water data. Their work focuses on history matching the early production data and using the results to estimate fracture properties.

Alkouh et al. (2013) argued that we cannot ignore the effect of gas flowing while analyzing water data which was the case in the previous work by Clarkson and Williams-Kovacs. Alkouh et al. (2013) introduced a new method to estimate the fracture effective volume using water flowback data while considering the effect of the gas flow.

They concluded that the total compressibility should be modified to account for gas compressibility.

In this work, we aim to modify Alkouh's method as we noticed that his method does not give accurate estimation to the effective fracture volume as will be shown in the next chapter.

CHAPTER III

WATER FLOWBACK IN GAS RESERVOIRS

This chapter will summarize the work done by Ahmad Alkouh in his PhD dissertation to estimate the fracture effective volume in shale gas wells. First, a description of the simulation model used by Alkouh (2014) will be presented. Alkouh (2014) showed a simulation case where his method gave a good estimation of the effective fracture volume. Several simulation cases will be run at different reservoir conditions in order to test Alkouh's method. A similar simulation model will be used in this work with different reservoir conditions. Then, we will apply Alkouh's method to estimate the fracture volume. The last section in this chapter will present a modification on Alkouh's method in order to have a more accurate estimation to the fracture effective volume in shale gas wells. A new method (modification of Alkouh's method) will be introduced in this chapter and it will be applied on field data in the next chapter.

3.1 Simulation Model

A single fracture simulation model is used. The fracture is filled with water while the matrix is filled with gas. The grids are geometrically spaced in order to capture the transient flow. Table 1 summarizes the properties used by Alkouh (2014) in his study. We used the same parameters as Alkouh (2014) did. Gas compressibility was obtained from Gasprop6 software using the initial reservoir pressure and temperature, and the gas gravity, Appendix A. The relative permeability curves for the simulation model are shown in Fig 7.

Table 1- Shale gas reservoir properties. Alkouh (2014)

Initial Pressure, p_i	3000 psi
Flowing bottom-hole pressure, p_{wf}	500 psi
Gas specific gravity, γ_g	0.65
Reservoir temperature, T	160 ^{o}F
Fracture porosity, φ_F	1.00 (fraction)
Water (Fracture) Volume, V_w	6,955 STB
Water formation volume factor, B_w	1.01 res bbl/STB
Matrix porosity, φ_m	0.06 (fraction)
Reservoir thickness, h	300 ft
Matrix permeability, k_m	1.5 x 10^{-4} md
Fracture spacing, L_F	500 ft
Fracture half length, x_F	550 ft
Formation compressibility, c_f	1.0 x 10^{-6} psi^{-1}
Water compressibility, c_w	2.9 x 10^{-6} psi^{-1}

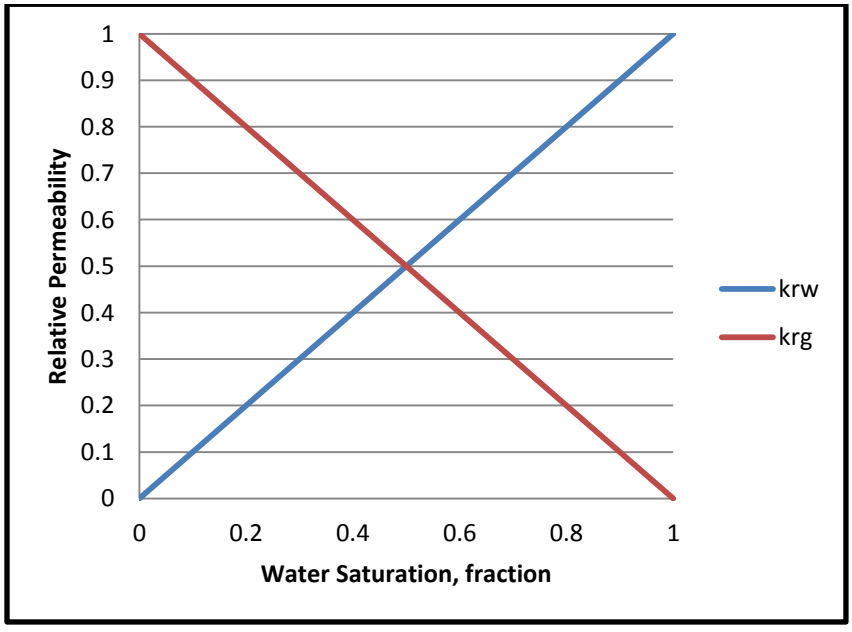

Fig 7. Relative permeability curves in the fracture system.

Two scenarios were tested using the described simulation model. The first scenario eliminates the gas flow from the matrix and only has water flowing from the fracture, Fig. 8. The second scenario allows gas to flow in order to observe its effect on water production data, Fig. 9. In both cases, water production data shows a ½ slope representing a fracture linear flow, Fig. 10. In addition, they both show a unit slope when water rate is plotted against water material balance time indicating that the boundary is felt, Fig.11.

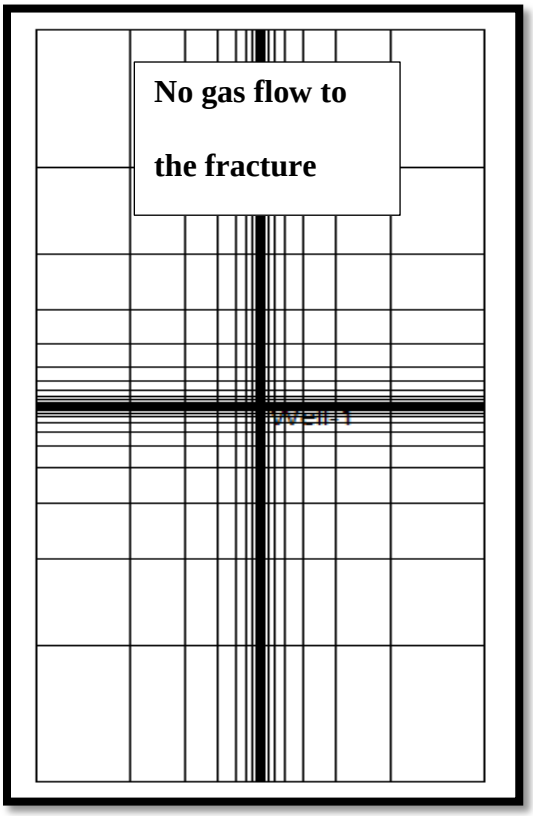

Fig. 8. Single phase flow is obtained where water is flowing in the fracture and no gas is allowed to flow from the matrix.

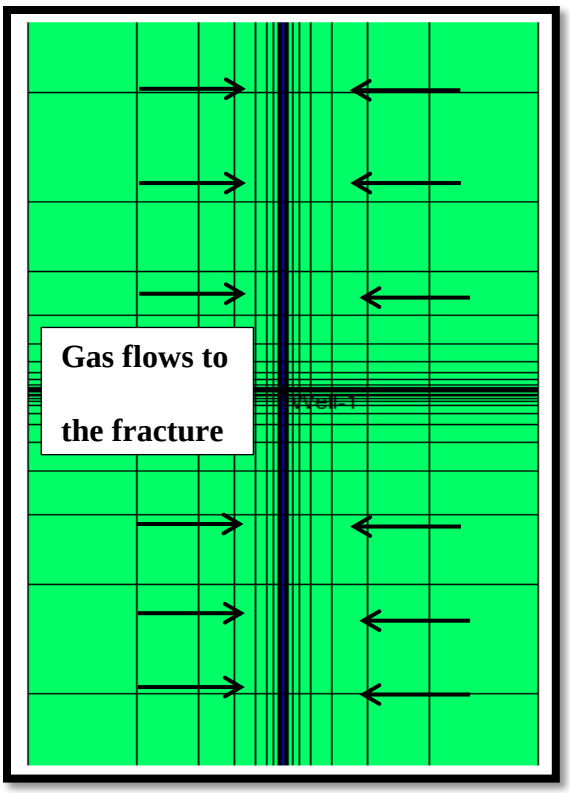

Fig. 9. Two phase flow is obtained where water is flowing in the fracture and gas is flowing from the matrix (green) to the fracture.

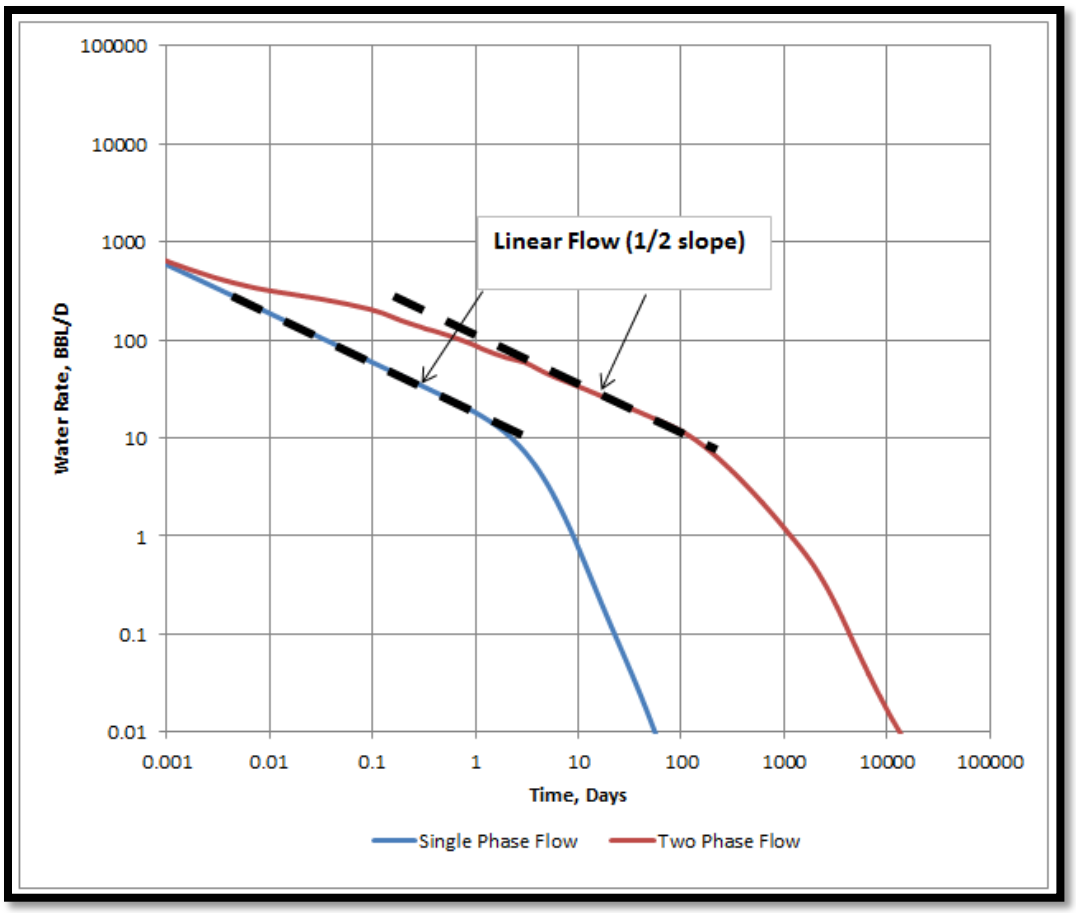

Fig. 10. Both the single phase case and the two phase case show a linear flow. However, the linear flow is delayed and shifted upward in the two phase case. This suggests that the gas compressibility is affecting the water production behavior.

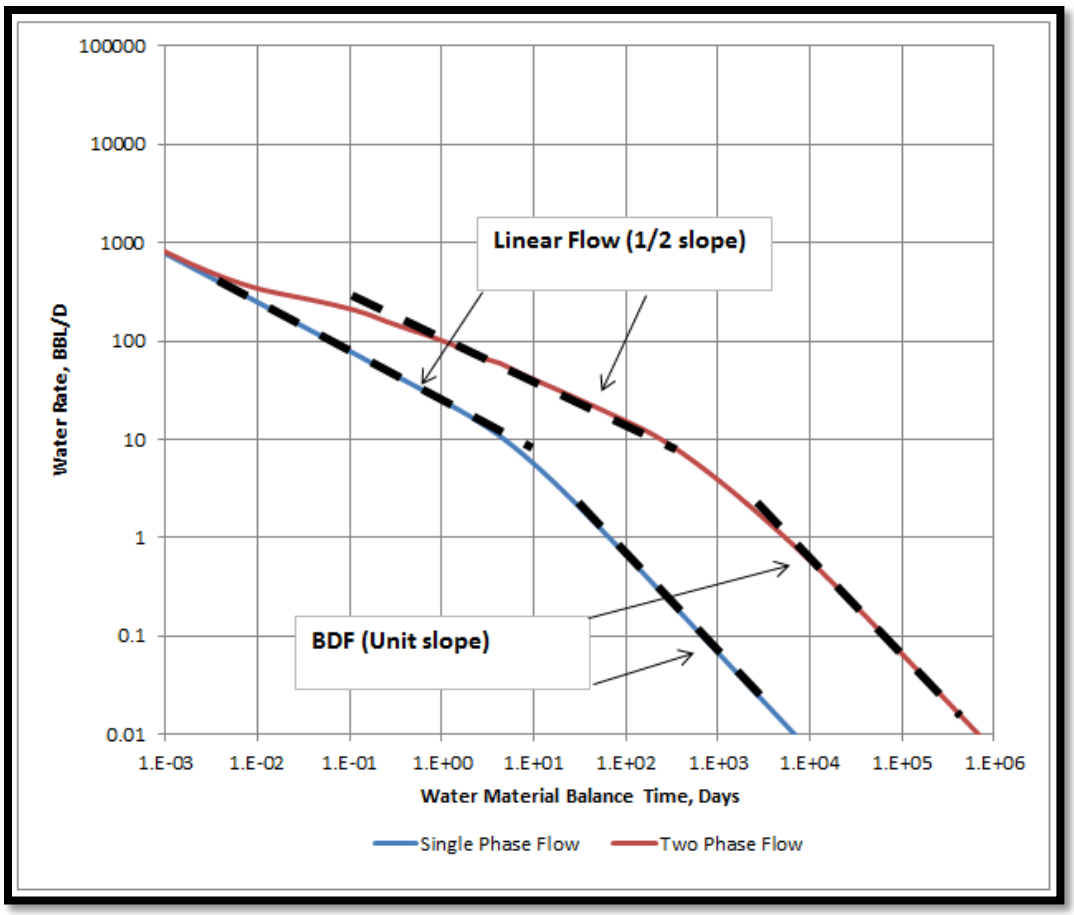

Fig.11. Both the single phase case and the two phase case show a linear flow and a boundary dominated flow (BDF). Similar to the previous figure, the water production data are shifted upward in the two phase case. This suggests that we have a larger water (fracture) volume while in fact we have the same water volume.

3.2 Estimating the Effective Fracture Volume in Shale Gas Wells

Alkouh's (2014) proposed a method to correct for the effect of gas production which gives a misleading result of having larger fracture volume by shifting the BDF line. His method aims to have a good estimation for the effective fracture volume using the water flowback data. He argued that the gas flow will affect the total compressibility

of the system and will dominate the diffusivity equation. Therefore, he suggested that water production data should be analyzed using the total compressibility (≈ gas compressibility) instead of water compressibility. The procedures of Alkouh's method to estimate the effective fracture volume are as follow:

1- Plot the water rate normalized pressure (RNP) vs. water material balance time. The pressure used to normalize the rate is equal to the difference between the initial pressure and the flowing bottom-hole pressure.
2- Identify the unit slope to ensure that the boundary is reached
3- Calculate the water volume using equations 3.1 and 3.2 where the total compressibility is calculated at the initial reservoir pressure with gas saturation, S_g, equals 1.

$$V_w = \frac{B_w}{c_t m_{pss}} \quad \ldots\ldots\ldots\ldots\ldots\ldots (3.1)$$

$$m_{pss} = \frac{RNP_w}{t_{mBw}} \quad \ldots\ldots\ldots\ldots\ldots\ldots (3.2)$$

By applying Alkouh's method on both the single phase case and the two phase case using Table 1 data, we get the results shown in Fig. 12, Fig. 13 and Fig.14.

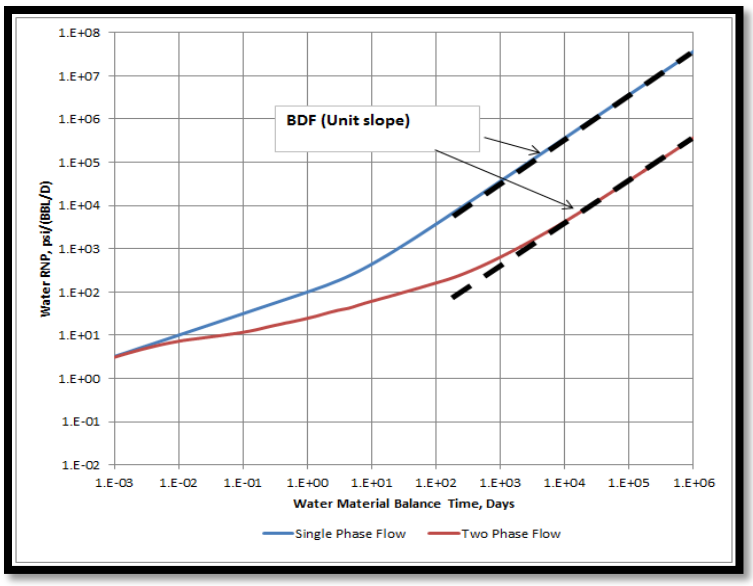

Fig. 12. Plotting water material balance vs. water rate normalized pressure shows a boundary in both cases. However, the two phase case unit slope is shifted downward indicating that we have a larger water volume than the single phase case.

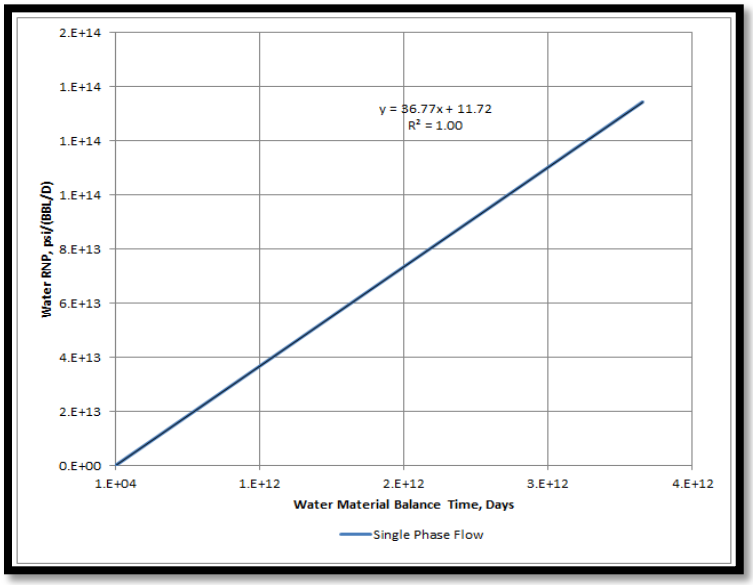

Fig. 13. The slope for the single phase case is calculated by plotting water material balance time vs. water rate normalized pressure on a Cartesian plot.

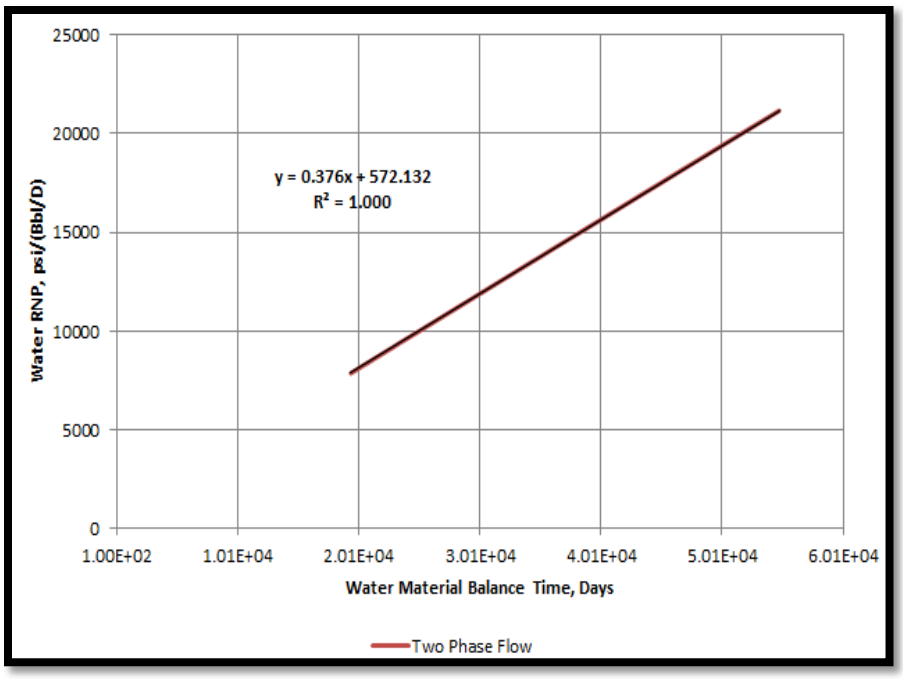

Fig.14. The slope for the two phase case is calculated by plotting water material balance time vs. water rate normalized pressure on a Cartesian plot.

After obtaining the values of m_{pss} for both cases, we apply Eq. 3.1 to estimate the fracture volume.

1- For single phase case:

$$V_w = \frac{B_w}{c_t m_{pss}} = \frac{1.01}{3.9 * 10^{-6} * 36.77} = 7{,}043\ STB$$

2- For two phase case with $(c_t \approx c_w + c_f)$

$$V_w = \frac{B_w}{c_t m_{pss}} = \frac{1.01}{3.9 * 10^{-6} * 0.376} = 688{,}762\ STB$$

3- For two phase case with $(c_t \approx c_{gi})$

$$V_w = \frac{B_w}{c_t m_{pss}} = \frac{1.01}{3.01 * 10^{-4} * 0.376} = 8{,}924\ STB$$

Alkouh's method ($c_t \approx c_{gi}$) gave good estimation to the effective fracture volume comparing with the case when water compressibility was used. However, Alkouh's method overestimated the volume by around 28%. When a gas compressibility of 3.9*10^{-4} psi^{-1} is then,

$$V_w = \frac{B_w}{c_t m_{pss}} = \frac{1.01}{3.918 * 10^{-4} * 0.376} = 6{,}856\ STB$$

In fact, a gas compressibility of 3.9*10^{-4} psi^{-1} is obtained at a pressure of 2,500 psi (the drawdown pressure), not the initial reservoir pressure (3,000 psi). This may suggest that the gas compressibility should be evaluated at the drawdown pressure. In order to confirm that conclusion, several simulation cases were run.

Since gas compressibility is mainly affected by temperature, gas gravity and pressure, those parameters will be altered and Alkouh's method will be applied on each simulation run to test its validity. In the simulation cases that will be run, the water volume will be estimated at different values of total compressibility. The first value will be equal to the gas compressibility at the initial reservoir pressure,c_{g_i}, as Alkouh (2014) suggested. The second value will be equal to the gas compressibility at the drawdown pressure, $c_{g_{DD}}$.

3.3 Sensitivity Study- Initial Reservoir Temperature

The first parameter that will be tested is the initial reservoir Temperature. Beside the base case discussed earlier, three cases will be run and the only variable will be initial reservoir temperature. Table 2 and Table 3 show the properties of the new cases.

Cases 1A-1C all show similar production profile and have similar values of m_{pss}, as shown in Fig. 15 and Fig. 16.

Table 2- Common reservoir properties for cases 1A-1C

Initial reservoir pressure, p_i	3,000 psi
Flowing bottom-hole pressure, p_{wf}	500 psi
Gas specific gravity, γ_g	0.65
Fracture porosity, φ_F	1.00
Water (Fracture) Volume, V_w	6,955 STB
Water formation volume factor, B_w	1.01 res bbl/STB
Matrix porosity, φ_m	0.06
Reservoir thickness, h	300 ft
Matrix permeability, k_m	1.5×10^{-4} md
Fracture spacing, L_F	500 ft
Fracture half length, x_F	550 ft
Formation compressibility, c_f	1.0×10^{-6} psi^{-1}
Water compressibility, c_w	2.9×10^{-6} psi^{-1}

Table 3- Initial reservoir temperature for cases 1A-1C.

Case	Temperature, ^{o}F	c_{g_i}, psi^{-1}	$c_{g_{DD}}$, psi^{-1}
Base Case	160	3.011×10^{-4}	3.918×10^{-4}
Case 1A	120	2.923×10^{-4}	3.909×10^{-4}
Case 1B	200	3.050×10^{-4}	3.901×10^{-4}
Case 1C	250	3.068×10^{-4}	3.873×10^{-4}

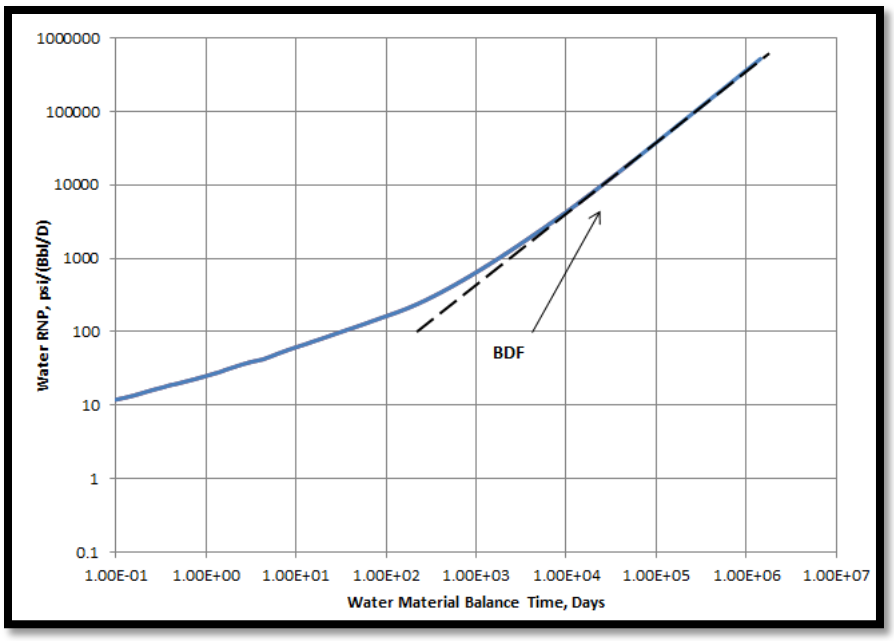

Fig. 15. Plotting water material balance vs. water rate normalized pressure shows a BDF in cases 1A-1C where their curves overlay each other (similar production profile).

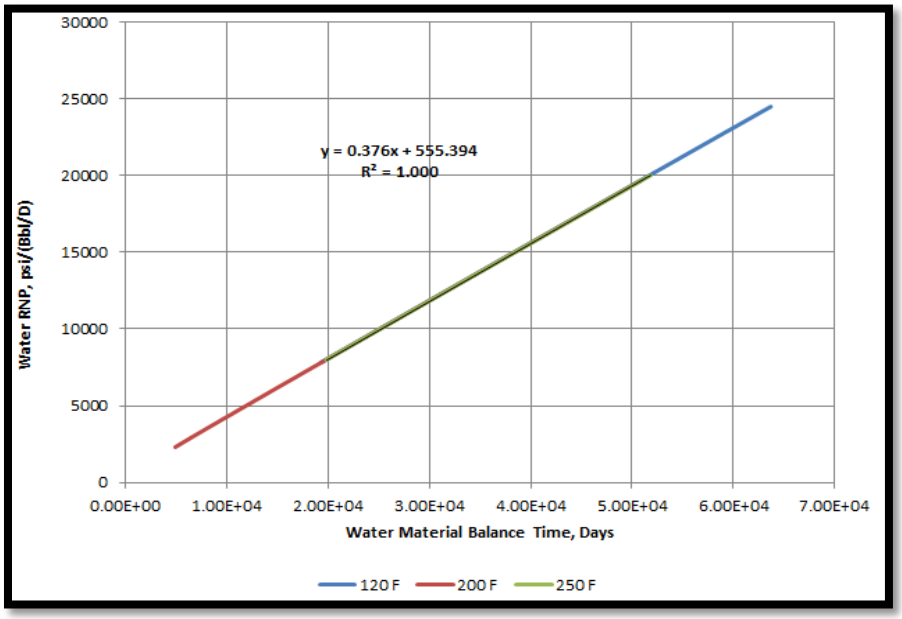

Fig. 16. The slope mpss is the same for cases 1A-1C and it equals 0.376.

3.3.1 Case 1A

The calculations of the base case are shown in the previous section. Therefore, we will start with the calculations of case 1A where the initial reservoir temperature is 120 ^{o}F. Fig. 15 shows the log-log plot of RNP vs. water material balance time. In addition, m_{pss} is determined from Fig. 16. Finally, we apply Eq. 3.1 as follows:

1- Alkouh's method ($c_t \approx c_{gi}$)

$$V_w = \frac{B_w}{c_t m_{pss}} = \frac{1.01}{2.923 * 10^{-4} * 0.376} = 9{,}190\ STB$$

2- ($c_t \approx c_{gDD}$)

$$V_w = \frac{B_w}{c_t m_{pss}} = \frac{1.01}{3.909 * 10^{-4} * 0.376} = 6{,}872\ STB$$

3.3.2 Case 1B

The calculations of case 1B where the initial reservoir temperature is 200 ^{o}F are as follows:

1- Alkouh's method ($c_t \approx c_{gi}$)

$$V_w = \frac{B_w}{c_t m_{pss}} = \frac{1.01}{3.05 * 10^{-4} * 0.376} = 8{,}807\ STB$$

2- ($c_t \approx c_{gDD}$)

$$V_w = \frac{B_w}{c_t m_{pss}} = \frac{1.01}{3.901 * 10^{-4} * 0.376} = 6{,}886\ STB$$

3.3.3 Case 1C

The calculations of case 1C where the initial reservoir temperature is 250 ^{o}F are as follows:

1- Alkouh's method ($c_t \approx c_{gi}$)

$$V_w = \frac{B_w}{c_t m_{pss}} = \frac{1.01}{3.068 * 10^{-4} * 0.376} = 8{,}755\ STB$$

2- ($c_t \approx c_{gDD}$)

$$V_w = \frac{B_w}{c_t m_{pss}} = \frac{1.01}{3.873 * 10^{-4} * 0.376} = 6{,}936\ STB$$

3.3.4 Discussion of Results- Cases 1A-1C

The results of the base case and cases 1A-1C are summarized in Table 4 and Fig. 17 . As seen, Alkouh's method does not account for the effect of the initial reservoir temperature which does not affect the water production behavior but it slightly affects the gas compressibility. This means that we will have different estimates of the effective fracture volume at different initial reservoir temperatures. However, the different estimates of the effective fracture volume will still be very close to each other and therefore we can ignore the effect of temperature on gas compressibility as Alkouh (2014) did.

Similar to the conclusion obtained from the base case, it appears that gas compressibility should be evaluated at the drawdown pressure instead of the initial pressure. Using $c_{g_{DD}}$provided volume estimations that are around 2% less than the actual

volume. In the other hand, using c_{g_i}overestimated the effective fracture volume by more than 25%.

Table 4 - Summary of results of cases 1A-1C

Case	Temperature	Actual fracture volume, STB	Alkouh's method estimation (c_{g_i}), STB	Estimation Using $c_{g_{DD}}$, STB
Base Case	160 ^{o}F	6,955	8,924	6,856
Case 1A	120 ^{o}F		9,190	6,872
Case 1B	200 ^{o}F		8,807	6,886
Case 1C	250 ^{o}F		8,755	6,936
Average			8,919	6,888
% Difference			+28.2%	1%

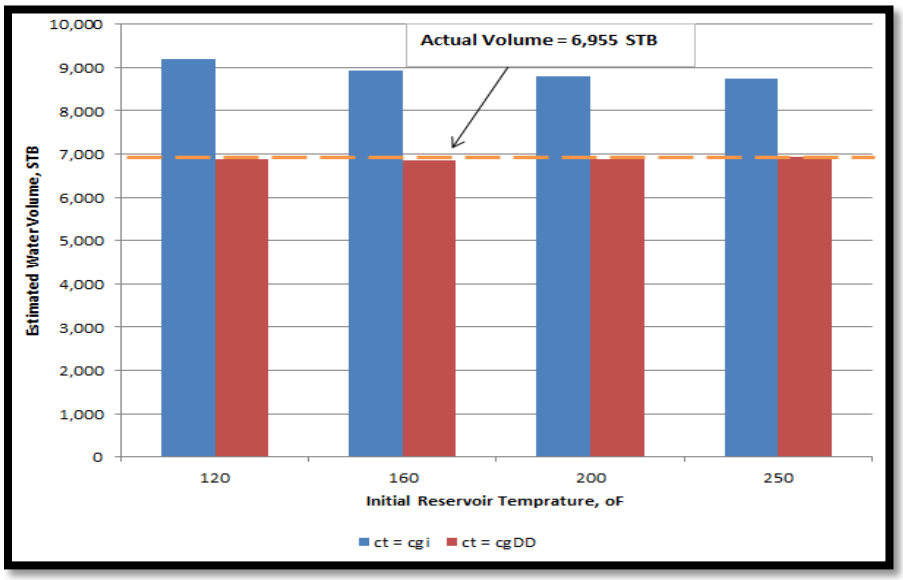

Fig. 17. Summary of the results of cases 1A-1C where Alkouh's method (Blue) overestimates the water volume while using gas compressibility at the drawdown pressure (red) would yield a good estimation of the actual water volume. Initial reservoir temperature does not have significant effect on the results.

3.4 Sensitivity Study- Gas Gravity

Similar to the sensitivity cases conducted on the initial reservoir temperature, the same cases were repeated but with changing the gas gravity and keeping the initial reservoir temperature constant. Table 5 and Table 6 show the properties of the new cases, 2A-2C.

Table 5 - Common reservoir properties for cases 2A-2C

Initial reservoir pressure, p_i	3,000 psi
Flowing bottom-hole pressure, p_{wf}	500 psi
Reservoir temperature, T	160 ^{o}F
Fracture porosity, φ_F	1.00
Water (Fracture) Volume, V_w	6,955 STB
Water formation volume factor, B_w	1.01 res bbl/STB
Matrix porosity, φ_m	0.06
Reservoir thickness, h	300 ft
Matrix permeability, k_m	1.5 x 10^{-4} md
Fracture spacing, L_F	500 ft
Fracture half length, x_F	550 ft
Formation compressibility, c_f	1.0 x 10^{-6} psi^{-1}
Water compressibility, c_w	2.9 x 10^{-6} psi^{-1}

Table 6 - Gas specific gravity for cases 2A-2C.

Case	Gas specific gravity, γ_g	c_{g_i}, psi^{-1}	$c_{g_{DD}}$, psi^{-1}
Base Case	0.65	3.011 x 10^{-4}	3.918 x 10^{-4}
Case 2A	0.55	3.090 x 10^{-4}	3.917 x 10^{-4}
Case 2B	0.7	2.944 x 10^{-4}	3.897 x 10^{-4}
Case 2C	0.8	2.736 x 10^{-4}	3.782 x 10^{-4}

Similar to cases 1A-1C, cases 2A-2C show similar production profiles and have similar values of m_{pss}, as shown in Fig. 18 and Fig. 19.

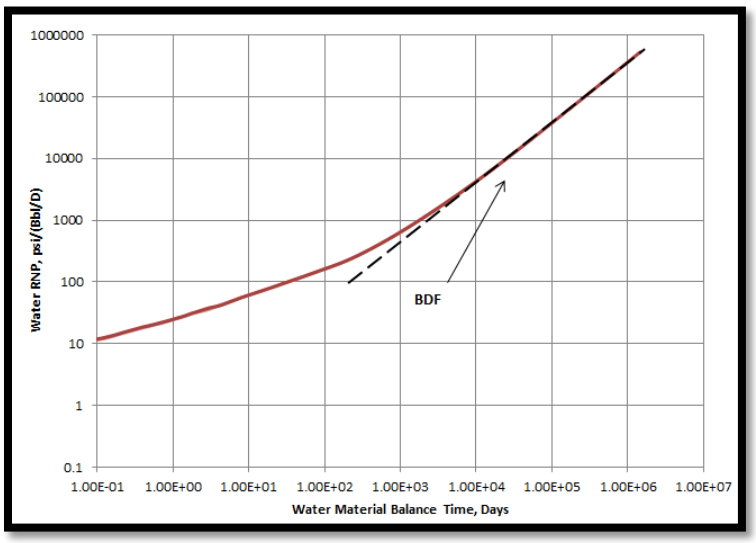

Fig. 18. Plotting water material balance vs. water rate normalized pressure shows a BDF in cases 2A-2C where their curves overlay each other (similar production profile).

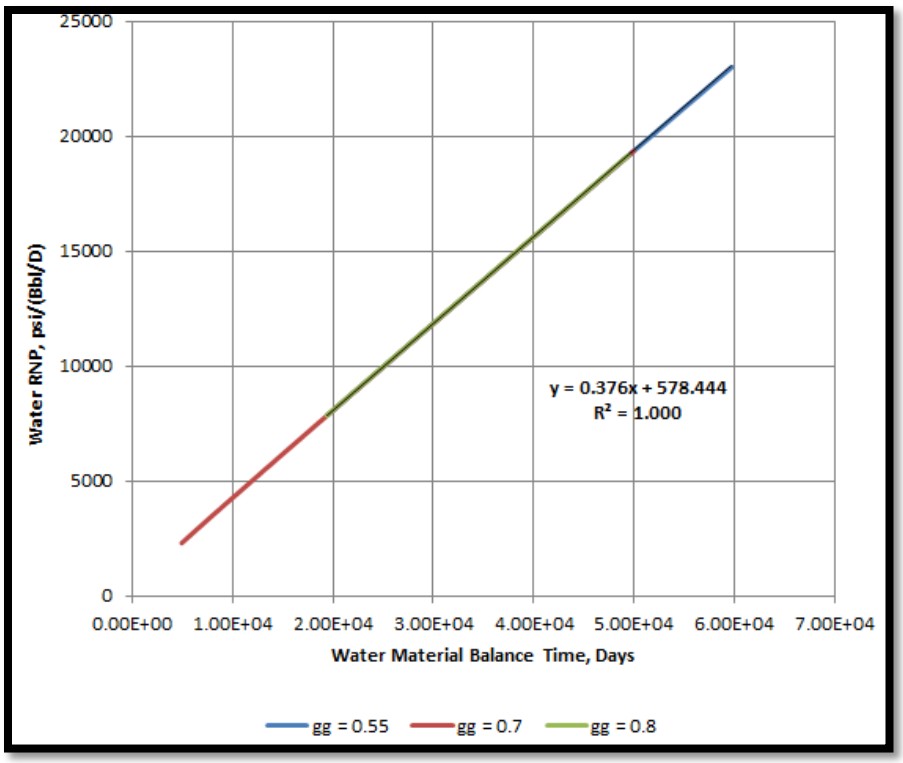

Fig. 19. The slope is the same for cases 2A-2C and it equals 0.376.

3.4.1 Case 2A

We start with the calculations of case 2A where the gas specific gravity is 0.55. Fig. 18 shows the log-log plot of RNP vs. water material balance time. In addition, m_{pss} is determined from Fig. 19. Finally, we apply Eq. 3.1 as follows:

3- Alkouh's method ($c_t \approx c_{gi}$)

$$V_w = \frac{B_w}{c_t m_{pss}} = \frac{1.01}{3.090 * 10^{-4} * 0.376} = 8{,}693\ STB$$

4- ($c_t \approx c_{gDD}$)

$$V_w = \frac{B_w}{c_t m_{pss}} = \frac{1.01}{3.917 * 10^{-4} * 0.376} = 6{,}858\ STB$$

3.4.2 Case 2B

The calculations of case 2B where the initial gas specific gravity is 0.7 are as follows:

3- Alkouh's method ($c_t \approx c_{gi}$)

$$V_w = \frac{B_w}{c_t m_{pss}} = \frac{1.01}{2.944 * 10^{-4} * 0.376} = 9{,}124\ STB$$

4- ($c_t \approx c_{gDD}$)

$$V_w = \frac{B_w}{c_t m_{pss}} = \frac{1.01}{3.897 * 10^{-4} * 0.376} = 6{,}893 STB$$

3.4.3 Case 2C

The calculations of case 2C where the initial gas specific gravity is 0.8 are as follows:

3- Alkouh's method ($c_t \approx c_{gi}$)

$$V_w = \frac{B_w}{c_t m_{pss}} = \frac{1.01}{2.736 * 10^{-4} * 0.376} = 9{,}818\ STB$$

4- ($c_t \approx c_{gDD}$)

$$V_w = \frac{B_w}{c_t m_{pss}} = \frac{1.01}{3.782 * 10^{-4} * 0.376} = 7{,}103\ STB$$

3.4.4 Discussion of Results- Cases 2A-2C

The results of cases 2A-2C are summarized in Table 7 and Fig. 20. Different gas gravities resulted in different estimates of the water volume. The difference would be large if Alkouh's method is used. For example, the difference between case 2A and case 2C is around 1,100 STB (≈16% of the actual water volume). If c_{gDD} is used, the difference would be small and negligible since all cases gave good estimates of the actual water volume. The cause of the different estimations is that gas gravity does not affect the water production profile while it does affect the gas compressibility and therefore would affect the estimation of the water volume if we use Eq. 3.1.

Similar to the conclusion obtained from the base case and cases 1A-1C, it seems that gas compressibility should be evaluated at the drawdown pressure instead of the initial pressure. Using $c_{g_{DD}}$provided volume estimations that are around 2% different than the actual volume. In the other hand, using c_{g_i}overestimated the effective fracture volume by more than 25%.

Table 7 - Summary of results of cases 2A-2C

Case	Gas gravity	Actual fracture volume, STB	Alkouh's method estimation (c_{g_i}), STB	Estimation Using $c_{g_{DD}}$, STB
Base Case	0.65	6,955	8,924	6,856
Case 2A	0.55		8,693	6,858
Case 2B	0.7		9,124	6,893
Case 2C	0.8		9,818	7,103
Average			9,206	6,932
% Difference			+31.4%	<1%

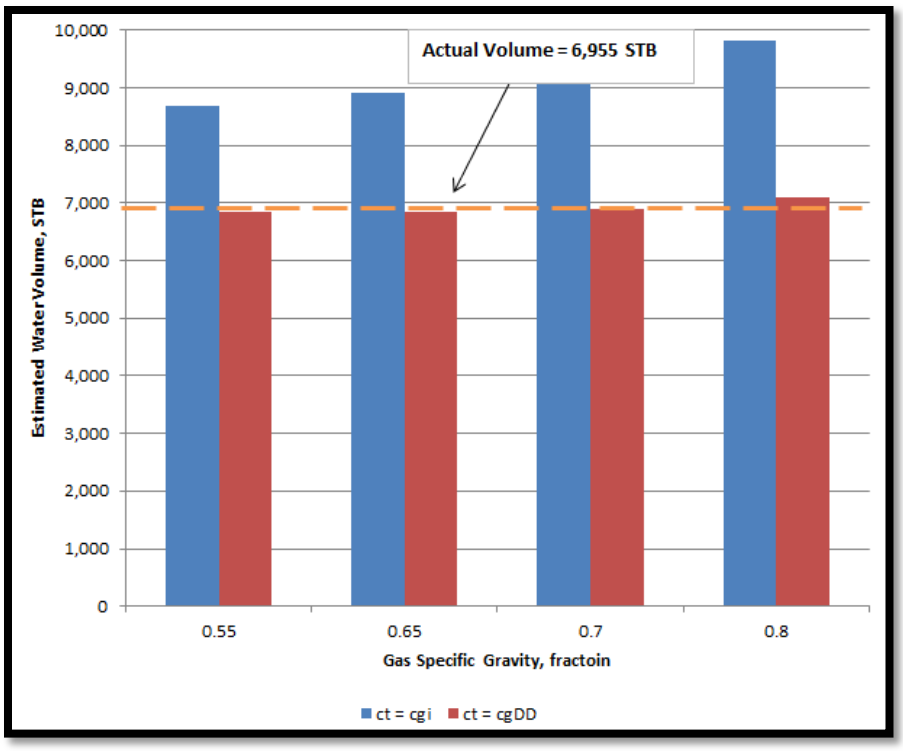

Fig. 20. Summary of the results of cases 2A-2C where Alkouh's method (Blue) overestimates the water volume while using gas compressibility at the drawdown pressure (red) would yield a good estimation of the actual water volume. Gas gravity would have some effect when using Alkouh's method while it would have a negligible effect when using cg_{DD}.

3.5 Sensitivity Study- Initial Reservoir Pressure

In the previous two sections, we have shown that evaluating the total compressibility at the drawdown pressure ($c_{g_{DD}}$) provides a very good estimation of the effective fracture volume regardless of both the initial reservoir temperature and the gas specific gravity which would have a slight effect on the volume estimation. The last parameter that affects the gas compressibility is pressure. Beside the base case, several sensitivity cases were run to understand the effect of pressure on the estimation of the

effective fracture volume. The first four cases are shown in this section whereas the remaining cases are discussed in the next sections. In this section we only change the initial reservoir pressure from 3,000 psi to 3,500 psi, 4,000 psi and 5,000 psi, respectively. The flowing bottom-hole pressure is held constant at 500 psi for all cases. All cases show a BDF (Fig. 21) and the slopes of each case are shown in Fig. 22 . Table 8 shows the compressibility values for each case.

Table 8 - Initial reservoir pressure for cases 3A-3D

Case	Pressure, psi	c_{g_i}, psi^{-1}	$c_{g_{DD}}$, psi^{-1}
Base Case	3,000	3.011×10^{-4}	3.918×10^{-4}
Case 3A	2,500	3.918×10^{-4}	5.202×10^{-4}
Case 3B	3,500	2.357×10^{-4}	3.011×10^{-4}
Case 3C	4,000	1.879×10^{-4}	2.357×10^{-4}
Case 3D	5,000	1.261×10^{-4}	1.526×10^{-4}

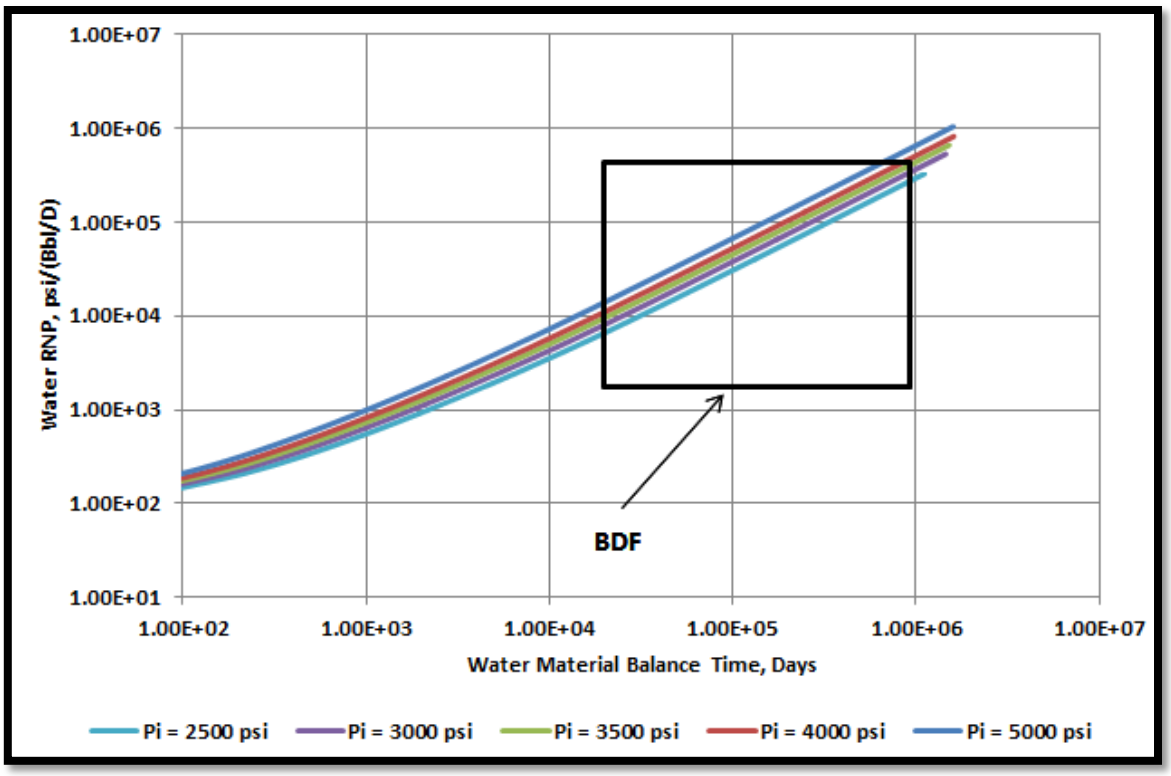

Fig. 21. Plotting water material balance vs. water rate normalized pressure shows a BDF in all the cases. However, as the initial pressure decreases, the curve is shifted downward indicating that we have larger water volumes while in fact we have the same water volume. This is expected since gas is more compressible at lower pressure values.

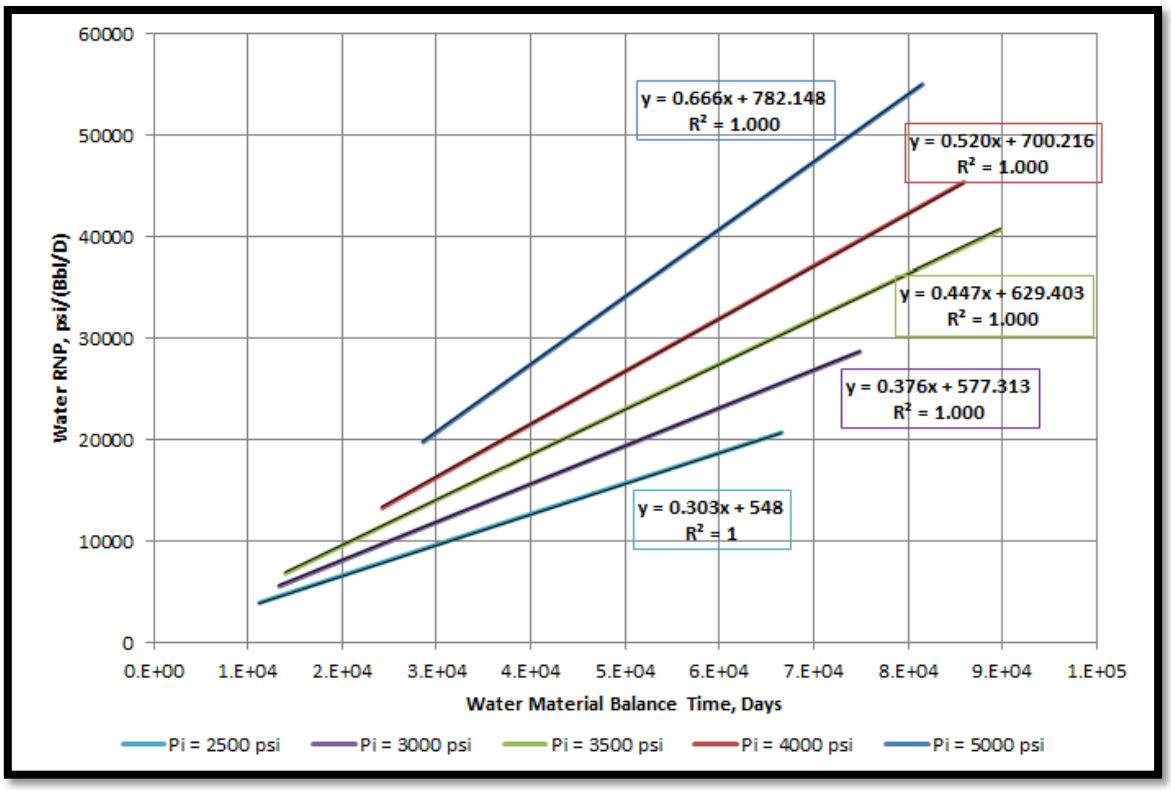

Fig. 22. The slope is the different for each case. Higher initial pressure values with the same flowing bottom-hole pressure result in higher values of the slope.

3.5.1 Case 3A

The calculations of the base case are shown in the previous section. Therefore, we will start with the calculations of case 3A where the initial reservoir pressure is 2,500 psi.

1- Alkouh's method ($c_t \approx c_{gi}$)

$$V_w = \frac{B_w}{c_t m_{pss}} = \frac{1.01}{3.918 * 10^{-4} * 0.303} = 8{,}508\ STB$$

2- ($c_t \approx c_{gDD}$)

$$V_w = \frac{B_w}{c_t m_{pss}} = \frac{1.01}{5.202 * 10^{-4} * 0.303} = 6{,}408\ STB$$

3.5.2 Case 3B

In this case, the initial reservoir pressure is 3,500 psi. By applying Eq. 3.1, we get the following results:

1- Alkouh's method ($c_t \approx c_{gi}$)

$$V_w = \frac{B_w}{c_t m_{pss}} = \frac{1.01}{2.357 * 10^{-4} * 0.447} = 9{,}586\ STB$$

2- ($c_t \approx c_{gDD}$)

$$V_w = \frac{B_w}{c_t m_{pss}} = \frac{1.01}{3.011 * 10^{-4} * 0.447} = 7{,}504\ STB$$

3.5.3 Case 3C

In this case, the initial reservoir pressure is 4,000 psi. By applying Eq. 3.1, we get the following results:

3- Alkouh's method ($c_t \approx c_{gi}$)

$$V_w = \frac{B_w}{c_t m_{pss}} = \frac{1.01}{1.879 * 10^{-4} * 0.52} = 10{,}337\ STB$$

4- ($c_t \approx c_{gDD}$)

$$V_w = \frac{B_w}{c_t m_{pss}} = \frac{1.01}{2.357 * 10^{-4} * 0.52} = 8{,}240\ STB$$

3.5.4 Case 3D

In this case, the initial reservoir pressure is 5,000 psi. By applying Eq. 3.1, we get the following results:

1- Alkouh's method ($c_t \approx c_{gi}$)

$$V_w = \frac{B_w}{c_t m_{pss}} = \frac{1.01}{1.261 * 10^{-4} * 0.666} = 12{,}026\ STB$$

2- ($c_t \approx c_{gDD}$)

$$V_w = \frac{B_w}{c_t m_{pss}} = \frac{1.01}{1.526 * 10^{-4} * 0.666} = 9{,}938\ STB$$

3.5.5 Discussion of Results- Cases 3A-3D

The results of the base case and cases 3A-3D are summarized in Table 9 and Fig. 23. Based on the results and calculations, it is obvious that changing the initial reservoir pressure will affect the accuracy of the effective fracture volume (water volume) estimation. As the gas compressibility decreases (higher initial reservoir pressure), both Alkouh's method and the new method ($c_t \approx c_{gDD}$) would yield higher values of the water volume. While Alkouh's method overestimated the water volume in all cases, the new method provided an accurate estimate when the initial reservoir pressure was 3,000 psi and it underestimated the volume at initial reservoir pressures below 3,000 psi and overestimated the volume at initial reservoir pressures above 3,000 psi. This is because the product of ($c_t m_{pss}$) is decreasing as we have higher initial pressure while maintaining the flowing bottom-hole pressure at a constant value, Fig. 24. Therefore, Eq.

3.1 should be multiplied by a constant to correct for the effect of changing ($c_t m_{pss}$). The value of the constant at different initial pressure values is obtained from Fig. 25.

Table 9 - Summary of results of cases 3A-3D

Case	Initial Reservoir Pressure, psi	Actual fracture volume, STB	Alkouh's method estimation (c_{g_i}), STB	Estimation Using $c_{g_{DD}}$, STB
Base Case	3,000	6,955	8,924	6,856
Case 3A	2,500		8,508	6,408
Case 3B	3,500		9,586	7,504
Case 3C	4,000		10,337	8,240
Case 3D	5,000		12,026	9,938
Average			9,876	7,789
% Difference			+42%	12%

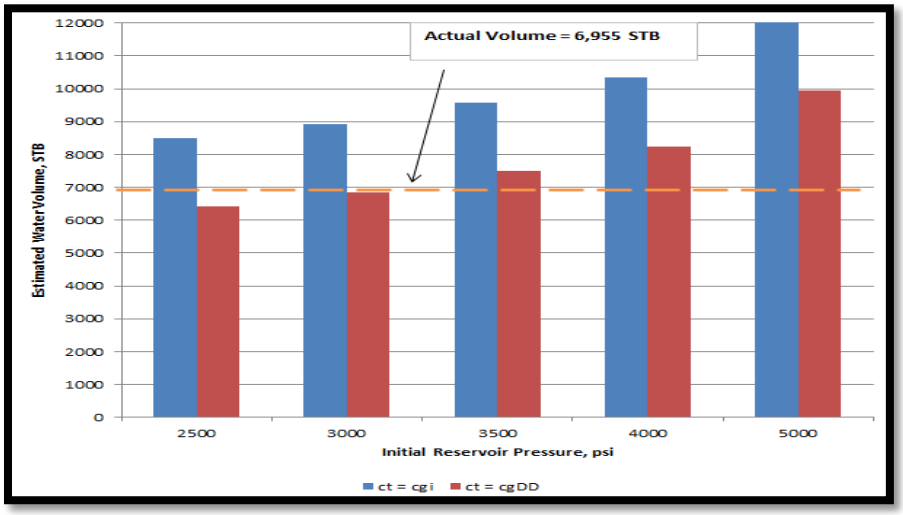

Fig. 23. Summary of the results of cases 3A-3D where Alkouh's method (Blue) overestimates the water volume in all the cases. Using gas compressibility at the drawdown pressure (red) will yield a good estimate of the actual water volume at initial pressure of 3,000 psi and will overestimate the volume at higher initial pressure values.

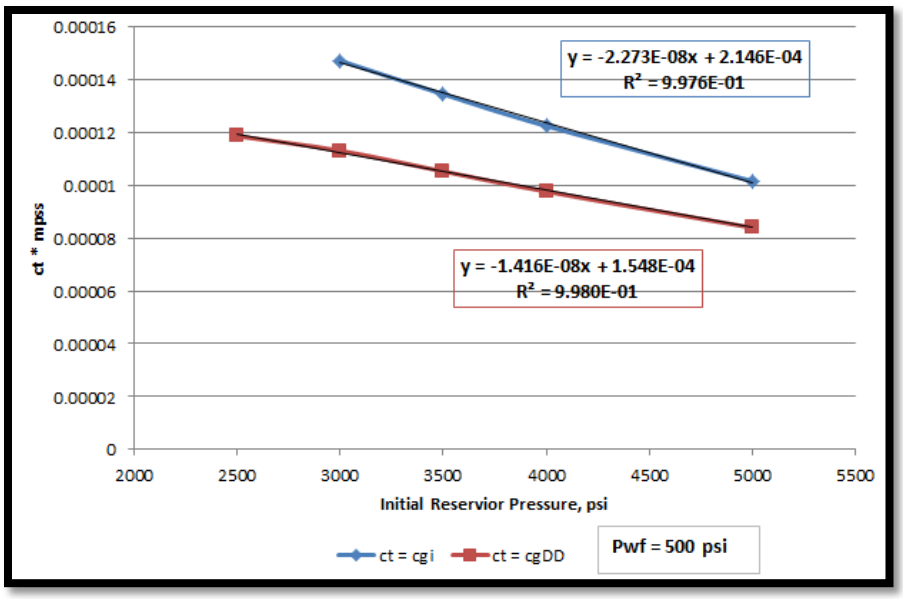

Fig. 24. The product of ct * m_{pss} is decreasing at higher initial reservoir pressure if the bottom-hole pressure is maintained constant. This will result in higher volume estimates at higher initial reservoir pressure which was shown in cases 3A-3D.

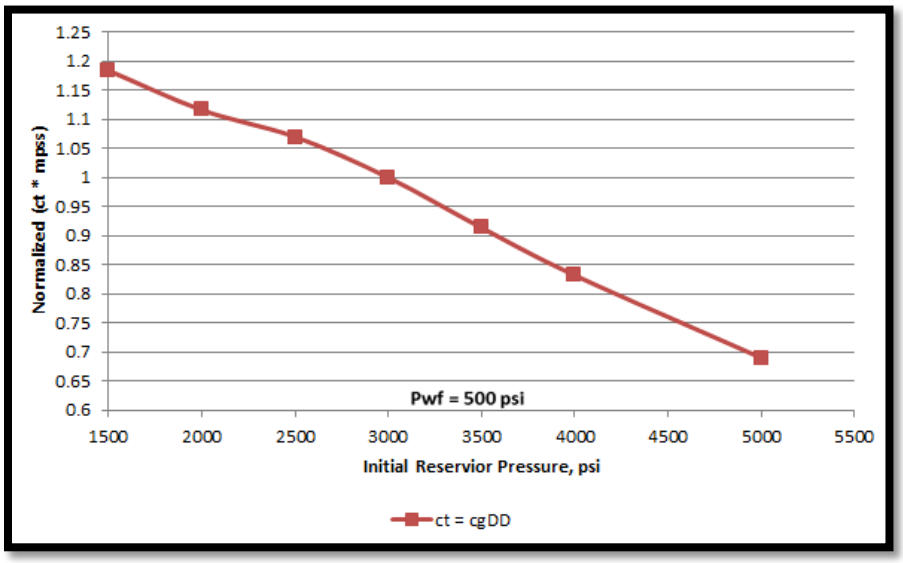

Fig. 25. The product of ct * m_{pss} is normalized by the product of ct * m_{pss} obtained when the initial pressure is 3,000 psi. This plot provide the constant that should be used to correct Eq. 3.1 when ct = cg_{DD}.

3.6 Sensitivity Study- Flowing Bottom-hole Pressure

The last parameter that will be tested in this study is the flowing bottom-hole pressure, p_{wf}. The results of six new cases will be discussed in this section and will be compared to three cases from the previous section in order to observe the effect of p_{wf} on the accuracy of the estimation of the effective fracture volume. The data of the new cases are summarized in Table 10. The water production profiles of the new cases are shown in Fig. 26, Fig. 28, and Fig. 30. In addition, the values of m_{pss} are shown in Fig. 27, Fig. 29, and Fig. 31.

Table 10 - Initial and flowing bottom-hole pressure for different cases

Case	Initial Pressure, psi	p_{wf}, psi	c_{g_i}, psi^{-1}	$c_{g_{DD}}$, psi^{-1}
Base Case	3,000	500	3.011×10^{-4}	3.918×10^{-4}
Case 4A		1,000		5.202×10^{-4}
Case 4B		1,500		7.149×10^{-4}
Case 3C	4,000	500	1.879×10^{-4}	2.357×10^{-4}
Case 4C		1,000		3.011×10^{-4}
Case 4D		1,500		3.918×10^{-4}
Case 3D	5,000	500	1.261×10^{-4}	1.526×10^{-4}
Case 4E		1,000		1.879×10^{-4}
Case 4F		1,500		2.357×10^{-4}

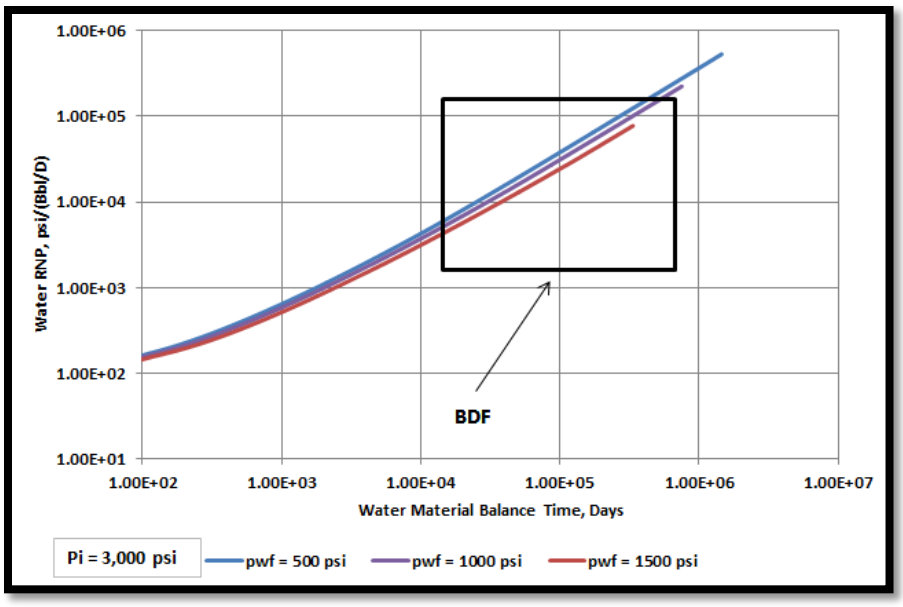

Fig. 26. Water RNP is plotted against water material balance time at different p_{wf} and constant initial reservoir pressure of 3,000 psi. Higher p_{wf} indicates higher water volumes while they are supposed to give the same volume.

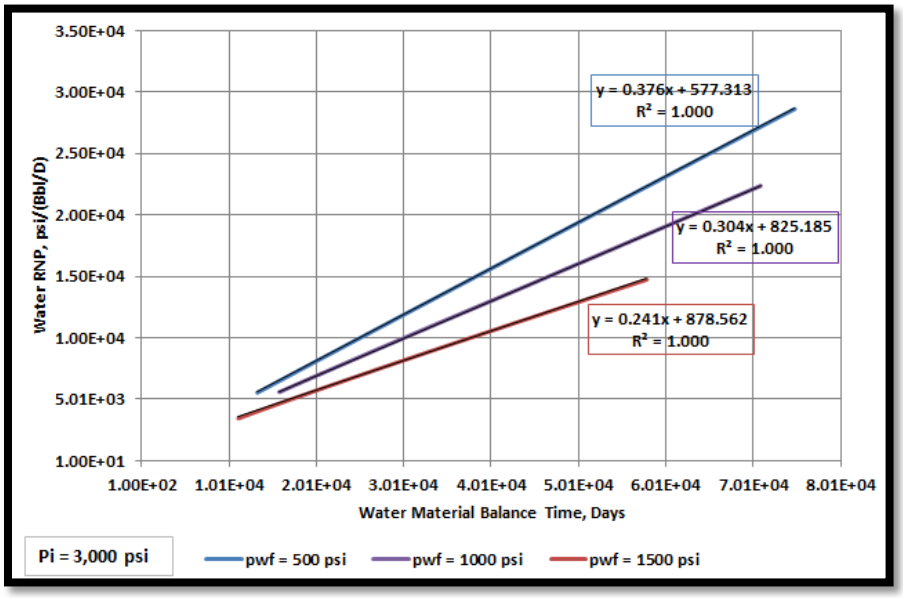

Fig. 27. The slope is different for each case. Higher p_{wf} pressure values with the same initial reservoir pressure of 3,000 psi will give lower values of m_{pss}.

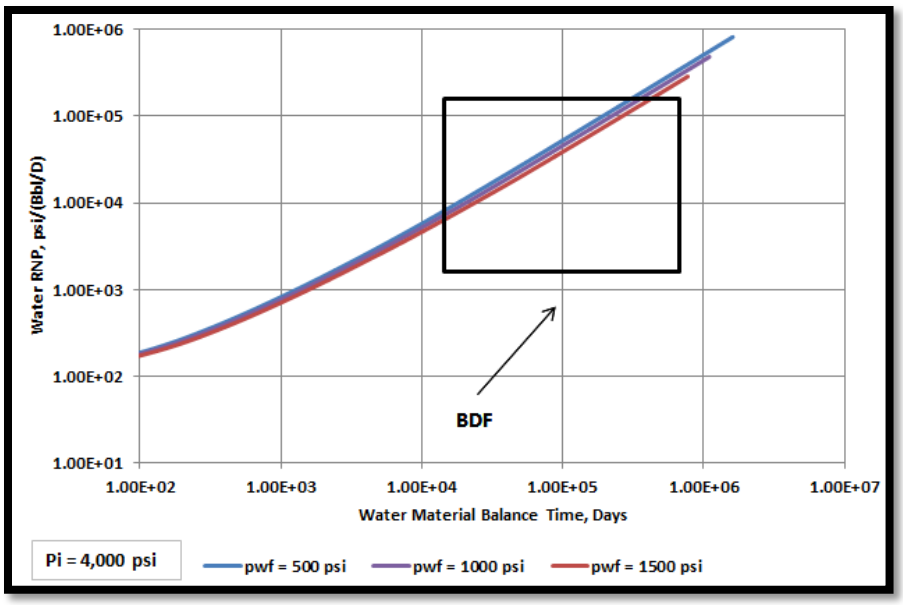

Fig. 28. Water RNP is plotted against water material balance time at different p_{wf} and constant initial reservoir pressure of 4,000 psi. Higher p_{wf} indicates higher water volumes while they are supposed to give the same volume.

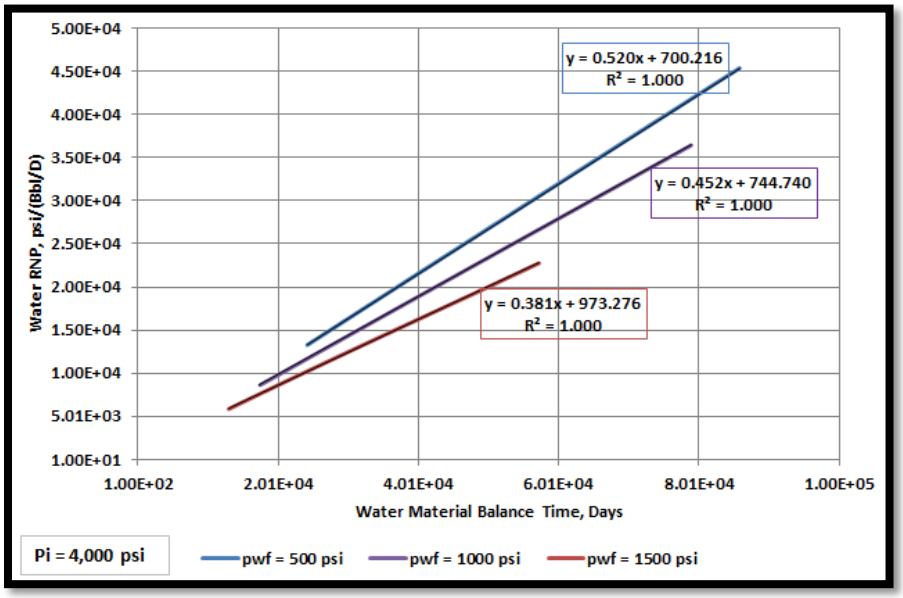

Fig. 29. The slope is different for each case. Higher p_{wf} pressure values with the same initial reservoir pressure of 4,000 psi will give lower values of m_{pss}.

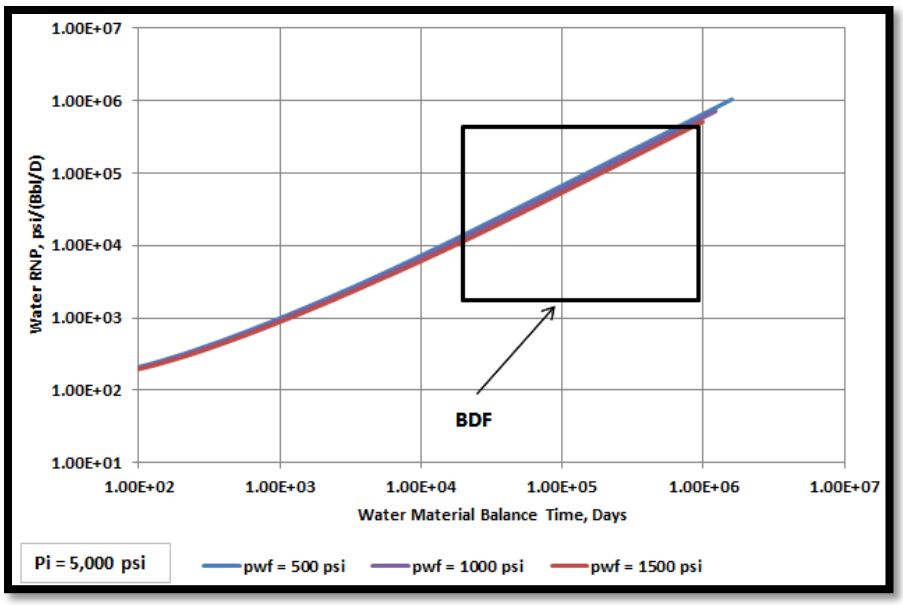

Fig. 30. Water RNP is plotted against water material balance time at different p_{wf} and constant initial reservoir pressure of 5,000 psi. Higher p_{wf} indicates higher water volumes while they are supposed to give the same volume.

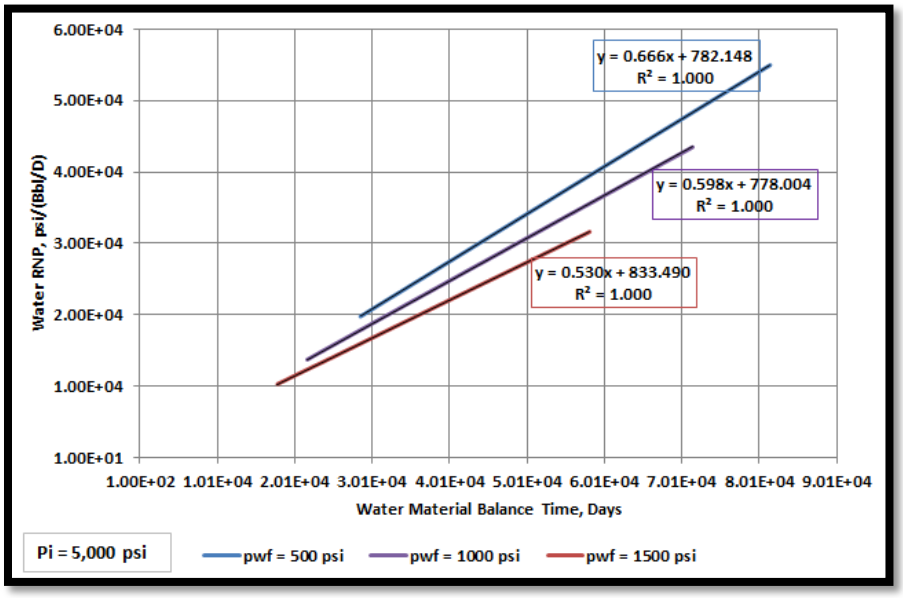

Fig. 31. The slope is different for each case. Higher p_{wf} pressure values with the same initial reservoir pressure of 5,000 psi will give lower values of m_{pss}.

3.6.1 Case 4A

The calculations of the base case, case 3C and case 3D are shown in the previous sections. Therefore, we will start with the calculations of case 4A where the initial reservoir pressure is 3,000 psi and p_{wf} is 1,000 psi.

3- Alkouh's method ($c_t \approx c_{gi}$)

$$V_w = \frac{B_w}{c_t m_{pss}} = \frac{1.01}{3.011 * 10^{-4} * 0.304} = 11{,}034\ STB$$

4- ($c_t \approx c_{gDD}$)

$$V_w = \frac{B_w}{c_t m_{pss}} = \frac{1.01}{5.202 * 10^{-4} * 0.304} = 6{,}387\ STB$$

3.6.2 Case 4B

In this case, the initial reservoir pressure is 3,000 psi and p_{wf} is 1,500 psi. By applying Eq. 3.1, we get the following results:

5- Alkouh's method ($c_t \approx c_{gi}$)

$$V_w = \frac{B_w}{c_t m_{pss}} = \frac{1.01}{3.011 * 10^{-4} * 0.241} = 13{,}918\ STB$$

6- ($c_t \approx c_{gDD}$)

$$V_w = \frac{B_w}{c_t m_{pss}} = \frac{1.01}{7.149 * 10^{-4} * 0.241} = 5862\ STB$$

3.6.3 Case 4C

In this case, the initial reservoir pressure is 4,000 psi and p_{wf} is 1,000 psi. By applying Eq. 3.1, we get the following results:

7- Alkouh's method ($c_t \approx c_{gi}$)

$$V_w = \frac{B_w}{c_t m_{pss}} = \frac{1.01}{1.879 * 10^{-4} * 0.452} = 11{,}892\ STB$$

8- ($c_t \approx c_{gDD}$)

$$V_w = \frac{B_w}{c_t m_{pss}} = \frac{1.01}{3.011 * 10^{-4} * 0.452} = 7{,}421\ STB$$

3.6.4 Case 4D

In this case, the initial reservoir pressure is 4,000 psi and p_{wf} is 1,500 psi. By applying Eq. 3.1, we get the following results:

3- Alkouh's method ($c_t \approx c_{gi}$)

$$V_w = \frac{B_w}{c_t m_{pss}} = \frac{1.01}{1.879 * 10^{-4} * 0.381} = 14{,}108\ STB$$

4- ($c_t \approx c_{gDD}$)

$$V_w = \frac{B_w}{c_t m_{pss}} = \frac{1.01}{3.918 * 10^{-4} * 0.381} = 6{,}766\ STB$$

3.6.5 Case 4E

In this case, the initial reservoir pressure is 5,000 psi and p_{wf} is 1,000 psi. By applying Eq. 3.1, we get the following results:

1- Alkouh's method ($c_t \approx c_{gi}$)

$$V_w = \frac{B_w}{c_t m_{pss}} = \frac{1.01}{1.261 * 10^{-4} * 0.598} = 13{,}394\ STB$$

2- ($c_t \approx c_{gDD}$)

$$V_w = \frac{B_w}{c_t m_{pss}} = \frac{1.01}{1.879 * 10^{-4} * 0.598} = 8{,}989\ STB$$

3.6.6 Case 4F

In this case, the initial reservoir pressure is 5,000 psi and p_{wf} is 1,500 psi. By applying Eq. 3.1, we get the following results:

1- Alkouh's method ($c_t \approx c_{gi}$)

$$V_w = \frac{B_w}{c_t m_{pss}} = \frac{1.01}{1.261 * 10^{-4} * 0.530} = 15{,}112\ STB$$

2- ($c_t \approx c_{gDD}$)

$$V_w = \frac{B_w}{c_t m_{pss}} = \frac{1.01}{2.357 * 10^{-4} * 0.530} = 8{,}085\ STB$$

3.6.7 Discussion of Results- Cases 4A-4F

The results of the base case and cases 4A-4D are summarized in Table 11 and Fig. 32. Based on the results and calculations, it is obvious that changing the flowing bottom-hole pressure will affect the accuracy of the effective fracture volume (water volume) estimation. Using Alkouh's method will overestimate the water volume in all cases and the difference will be greater as we increase the p_{wf}. This is because we are normalizing the rate using lower value of ($Pi - p_{wf}$) which will reduce the value of the slope (m_{pss}) while the gas compressibility will be the same. The new method resulted in much better estimates of the water volume especially at lower pressure and lower flowing bottom-hole pressure. In contrast to Alkouh's method, increasing p_{wf} will result

in lower water volume estimation. This is because c_{gDD} is changing in each case and the product of $(c_{gDD}\ m_{pss})$ is increasing at higher p_{wf}, Fig. 33. Therefore, Eq. 3.1 should be multiplied by a constant to correct for the effect of changing $(c_{gDD}\ m_{pss})$. The value of the constant at different p_{wf} values can be obtained from Fig. 34.

Table 11 - Summary of results of cases 4A-4F

Case	Initial Reservoir Pressure, psi	p_{wf}, psi	Actual fracture volume, STB	Alkouh's method estimation (c_{g_i}), STB	Estimation Using $c_{g_{DD}}$, STB
Base Case	3,000	500	6,955	8,924	6,856
Case 4A		1,000		11,034	6,387
Case 4B		1,500		13,918	5,862
Case 3C	4,000	500		10,337	8,240
Case 4C		1,000		11,892	7,421
Case 4D		1,500		14,108	6,766
Case 3D	5,000	500		12,026	9,938
Case 4E		1,000		13,394	8,989
Case 4F		1,500		15,112	8,085
Average				12,305	7,606
% Difference				+76.9%	+9.5%

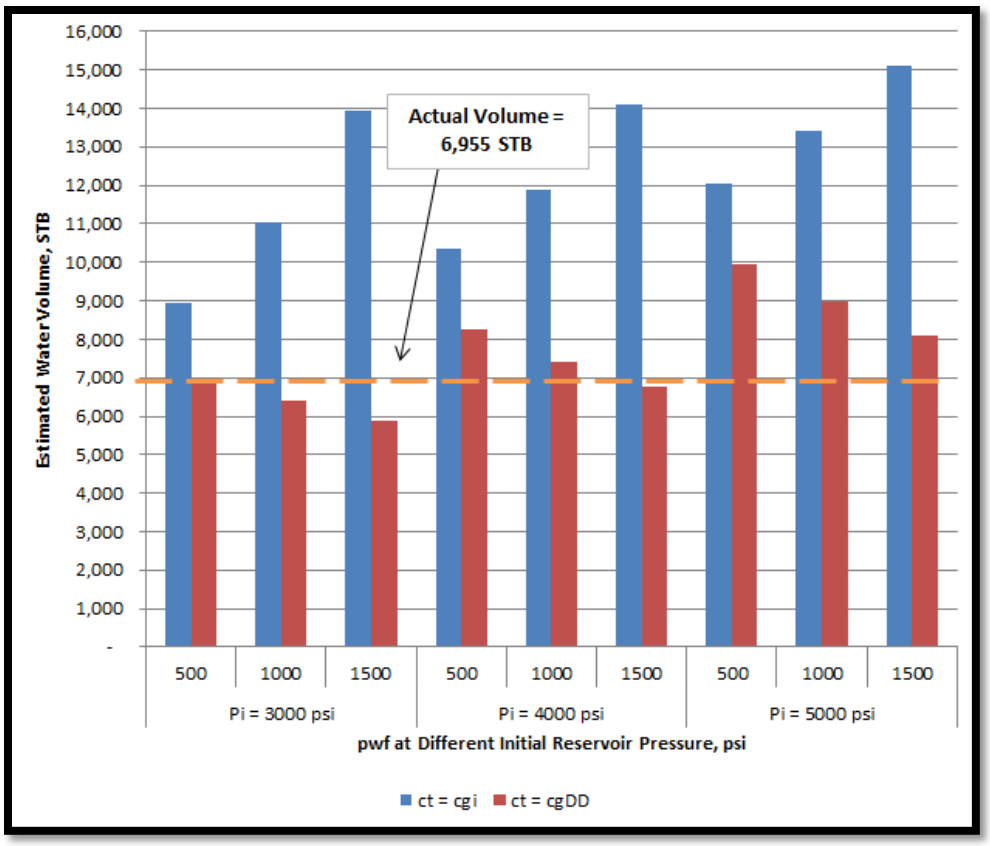

Fig. 32. Summary of the results of cases 4A-4F where Alkouh's method (Blue) overestimates the water volume in all the cases. In addition, as the pwf increases at the same initial reservoir pressure, Alkouh's method gave higher water volumes. This is due to the decrease in the value of product of (cgi * mpss) as pwf increase where cgi will remain constant while ($P_i - p_{wf}$) will decrease. On the other hand, using gas compressibility at the drawdown pressure (red) would yield much better estimates especially at lower initial pressure values (3,000 -4,000 psi). In addition, increasing p_{wf} at the same initial pressure will result in lower water volume estimates. This is because the product of ($cg_{DD} * m_{pss}$) is increasing as pwf increases.

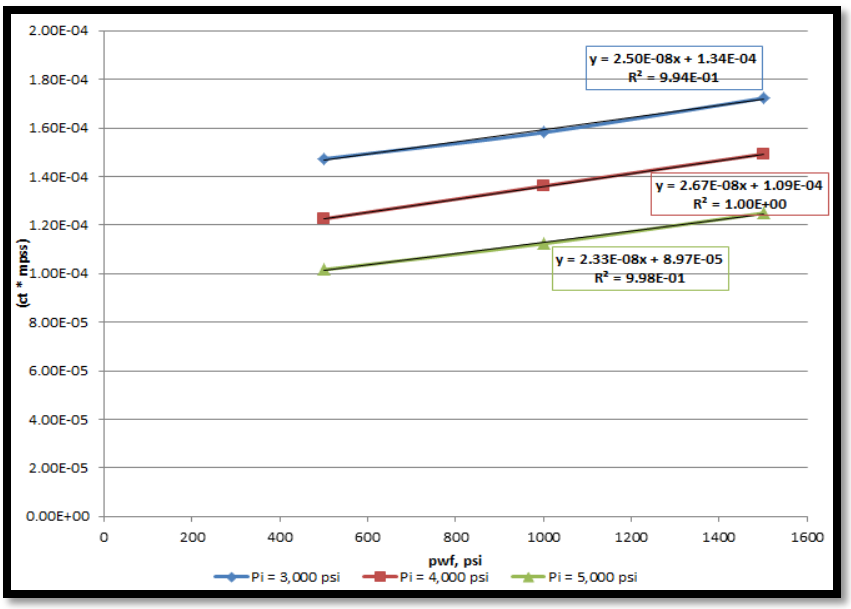

Fig. 33. The product of ct * m_{pss} is increasing at higher pwf if ct = cg_{DD}. This will result in lower volume estimation at higher p_{wf} which was shown in cases 4A-4F.

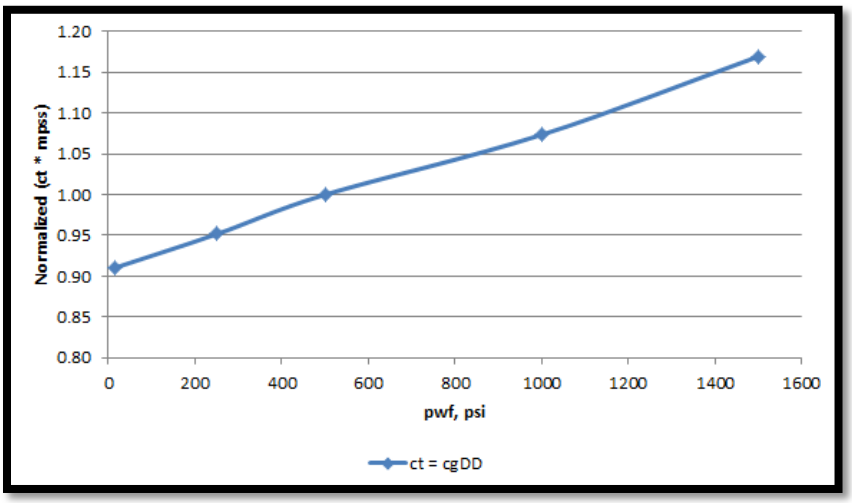

Fig. 34. The product of ct * m_{pss} is normalized by the product of ct * m_{pss} obtained when p_{wf} is 500 psi. This plot provides the constant that should be used to correct Eq. 3.1 when ct = cg_{DD}. Although this plot is based on the cases with an initial pressure of 3,000 psi, it still gives a good approximation at different initial reservoir pressures.

3.7 Summary

In this chapter, the simulation model was discussed and Alkouh's method of estimating the effective fracture volume was discussed in details. Several simulation cases were analyzed to identify the effect of different parameters on the gas compressibility and test Alkouh's method. It was concluded that neither the gas gravity nor the reservoir temperature would have a significant effect on the gas compressibility and therefore their effect can be ignored. In the other hand, both initial reservoir pressure and flowing bottom-hole pressure have significant effect on the product of $(c_t\, m_{pss})$ and therefore a modification on Alkouh's method was proposed.

First, it is recommended to use $(c_t = c_{gDD})$ instead of $(c_t = c_{gi})$ which was proposed by Alkouh (2014). In addition, we introduced normalizing plots that would provide constants to correct Eq. 3.1. as follows:

$$V_w = \frac{B_w}{c_{gDD} m_{pss}} * C_1 * C_2 \qquad \ldots\ldots\ldots\ldots\ldots\ldots (3.3)$$

Where,

C_1 and C_2 are constant to correct for the variable initial reservoir pressure and the variable flowing bottom-hole pressure and can be obtained from Fig. 25 and Fig. 34. Table 12 and Fig. 35 show a summary of different cases where the new method (Eq. 3.3) was used. The new method showed very good estimates of the effective fracture volume with a maximum difference of around 6% which occurs at the highest pressure and highest p_{wf}.

Table 12 - Summary of results of cases 4A-4F using the new method

Case	Initial Reservoir Pressure, psi	p_{wf}, psi	Actual fracture volume, STB	Estimation Using $Eq.$ 3.3, STB
Base Case	3,000	500	6,955	6,856
Case 4A		1,000		6,834
Case 4B		1,500		6,859
Case 3C	4,000	500		6,856
Case 4C		1,000		6,606
Case 4D		1,500		6,586
Case 3D	5,000	500		6,857
Case 4E		1,000		6,637
Case 4F		1,500		6,527
Average				6,735
% Difference				-3.2%

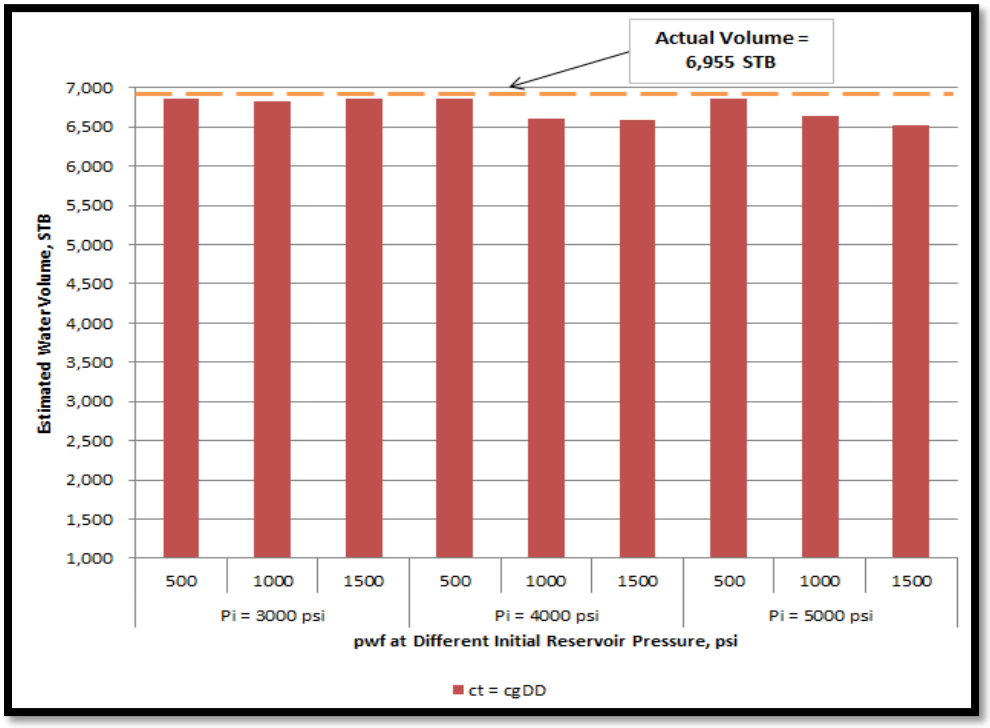

Fig. 35. Summary of the results of cases 4A-4F where the new method provides a very good estimate of the water volume in all cases.

CHAPTER IV

FIELD EXAMPLES

In this chapter, four gas wells from Fayetteville reservoir will be analyzed to test the new method introduced in the previous chapter.

4.1 Field Examples

Beside the water production rate, both P_i and p_{wf} should be known to use Eq. 3.3. The first well analyzed was FF-1, the same well Alkouh (2014) analyzed in his PhD dissertation.

4.1.1 FF-1

Fig. 36 shows the water production rate vs. time. The rate is normalized by dividing it by $(P_i - p_{wf})$ in order to get water RNP. Then, m_{pss} and $c_{gDD}$are estimated. Finally, the water volume is calculated using Eq. 3.3. Fig.37, Fig. 38, and Fig. 39 are used to estimate the effective fracture volume. The well data and results are summarized in Table 13.

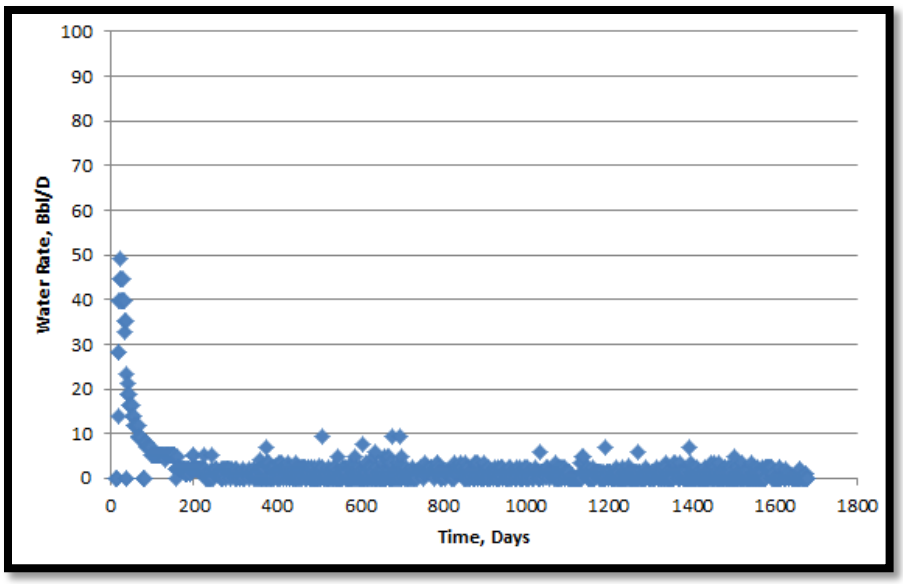

Fig. 36. FF-1 Decline curve plot of water rate vs. time.

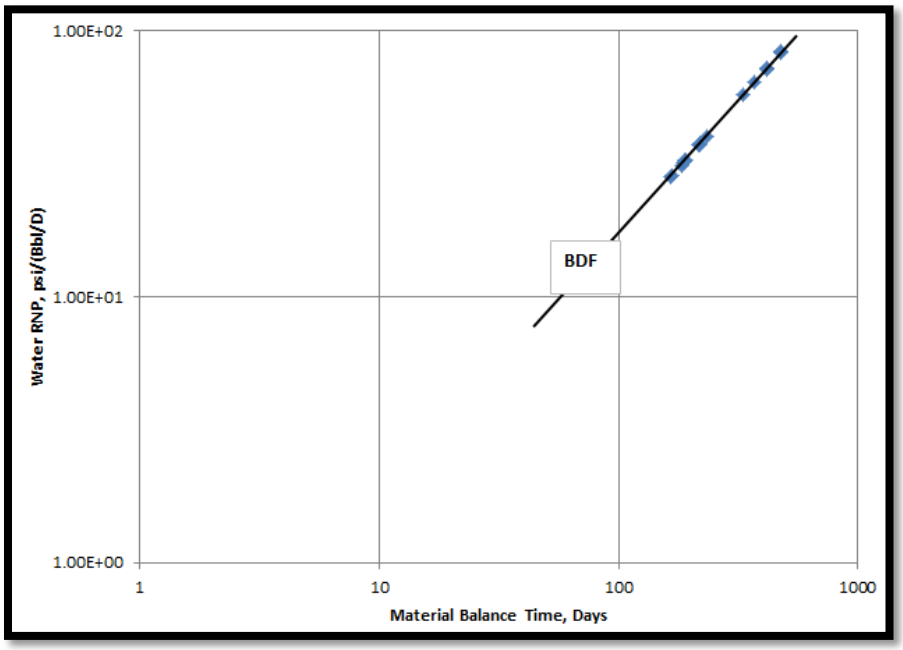

Fig.37. FF-1 reached BDF immediatly after the well was put in production.

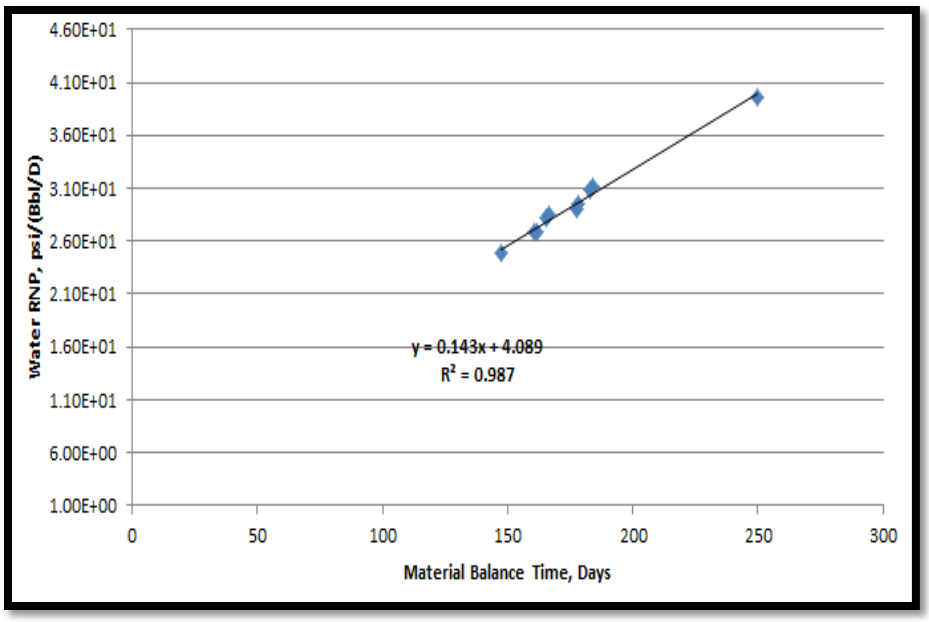

Fig. 38. m_{pss} for FF-1 is 0. 143 and it is obtained after 10 days of production.

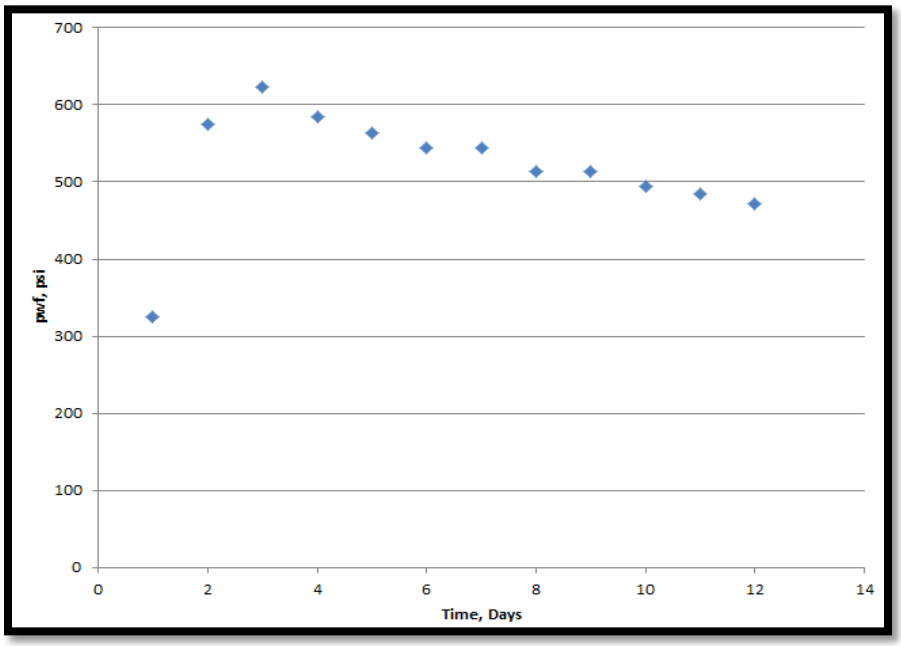

Fig. 39. The average flowing bottom-hole pressure for FF-1 is around 500 psi for the analyzed period (2-12 days).

Table 13 - Estimation of effective fracture volume for FF-1

Initial reservoir pressure	1,736 psi
Gas gravity	0.58
Reservoir temperature	118 ^{o}F
Cumulative injected water	72,642 Bbl
Cumulative produced water after around 4.5 years	10,167 Bbl
m_{pss}	0. 143 $\frac{psi}{Bbl}$
Average flowing bottom-hole pressure in the first 15 days	500 psi
c_{gDD}(at 1236 psi)	8.707 * 10^{-4} psi^{-1}
C1 and C2 for Eq. 3.3	1.15 and 1.00
Calculated Water Volume	9,200 Bbl = 12.7 % of injected water

4.1.2 FF-4

We follow the same procedures as we did in FF-1. Fig. 40, Fig.41, Fig. 42, and Fig. 43 are used to perform our analysis and estimate the effective fracture volume. The calculations for FF-4 are shown in Table 14.

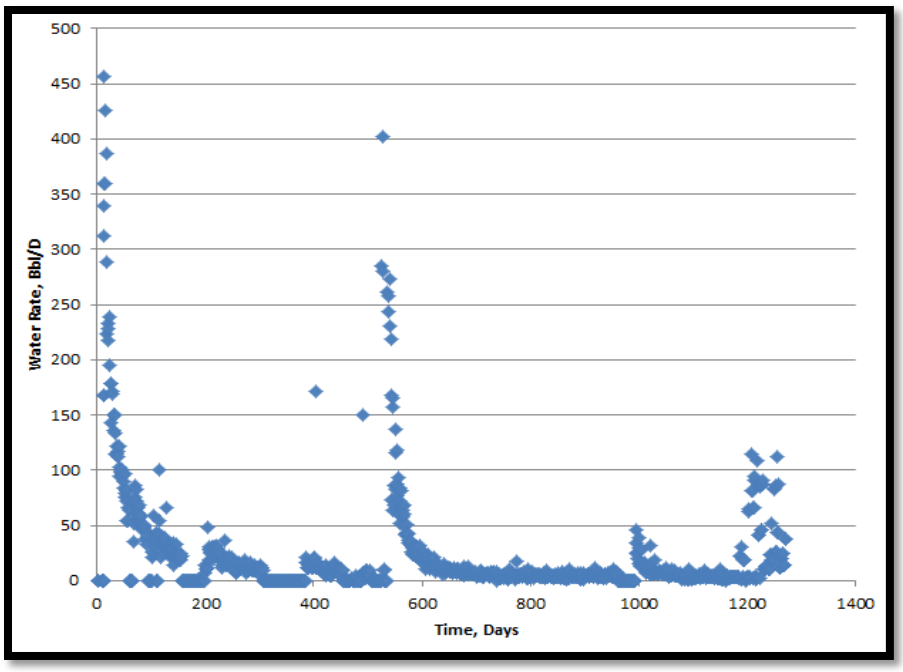

Fig. 40. FF-4 Decline curve plot of water rate vs. time.

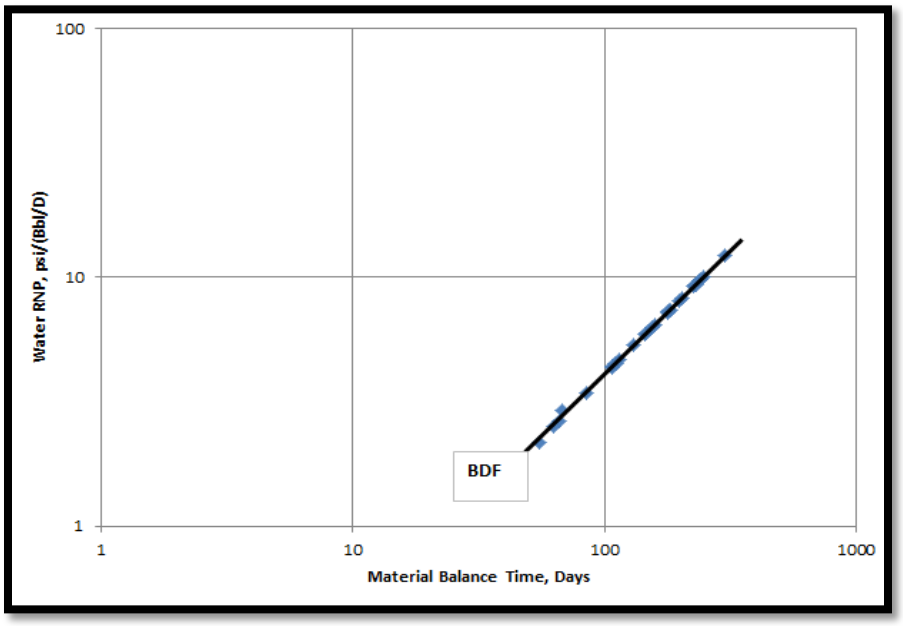

Fig.41. FF-4 reached BDF immediatly after the well was put in production.

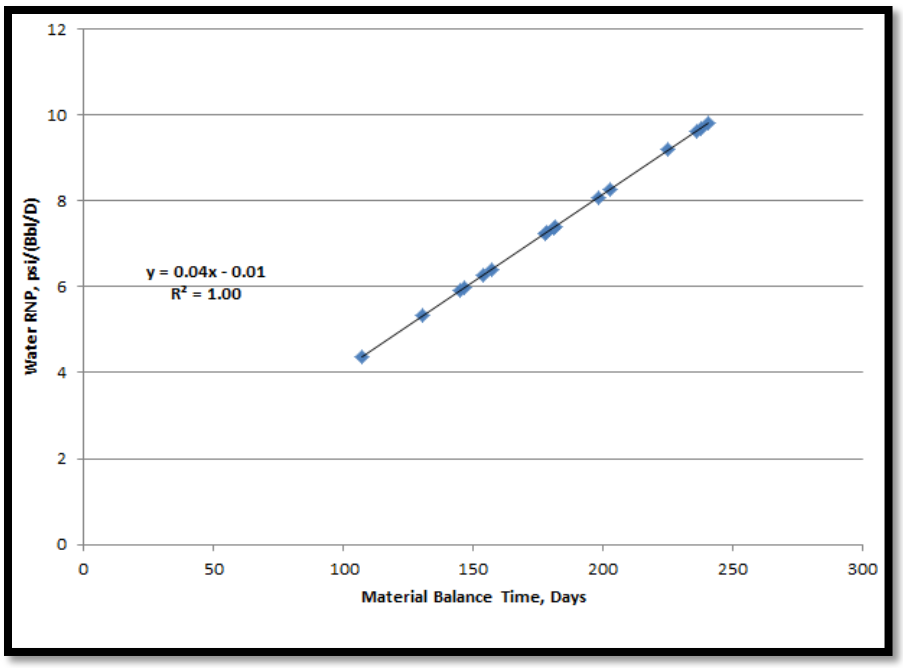

Fig. 42. m_{pss} for FF-4 is 0. 04 and it is obtained after 15 days of production.

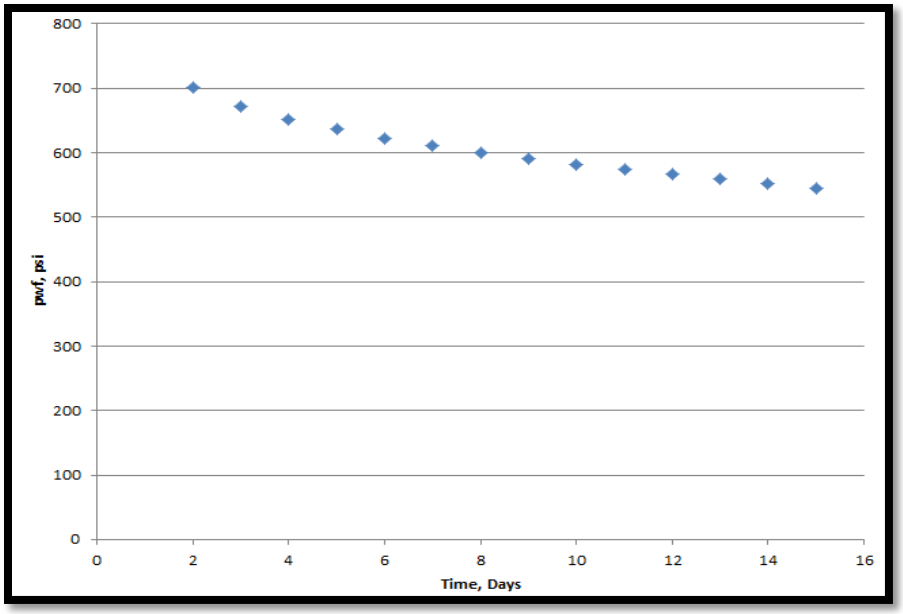

Fig. 43. The average flowing bottom-hole pressure for FF-4 is around 600 psi for the analyzed period (2-15 days).

Table 14 - Estimation of effective fracture volume for FF-4

Initial reservoir pressure	1,736 psi
Gas gravity	0.58
Reservoir temperature	118 ^{o}F
Cumulative injected water	158,790 Bbl
Cumulative produced water after around 1.3 years	35,491 Bbl
m_{pss}	0.04 $\frac{psi}{Bbl}$
Average flowing bottom-hole pressure in the analyzed period	600 psi
c_{gDD}(at 1136 psi)	9.494 * 10^{-4} psi^{-1}
C1 and C2 for Eq. 3.3	1.15 and 1.03
Calculated Water Volume	31,501 Bbl = 19.8 % of injected water

4.1.3 FF-5

Table 15 summarizes the results for FF-5. Fig 44, Fig.45, Fig. 46, and Fig. 47 are used to perform our analysis and estimate the effective fracture volume.

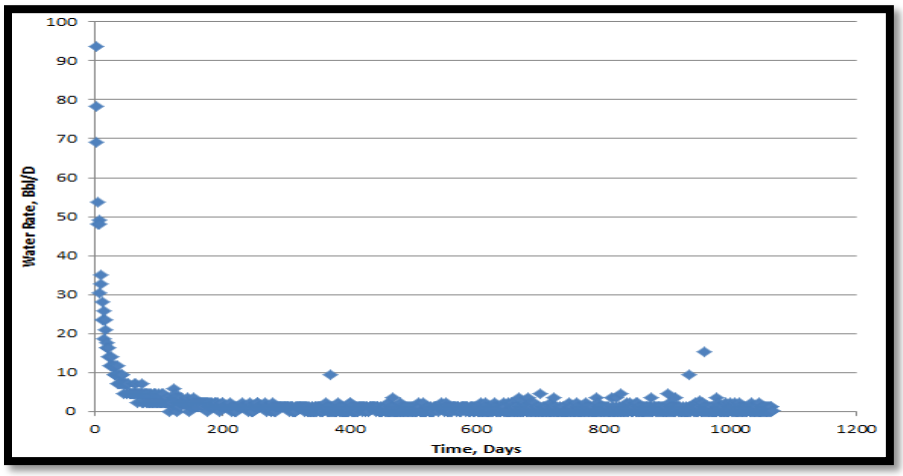

Fig 44. FF-5 Decline curve plot of water rate vs. time.

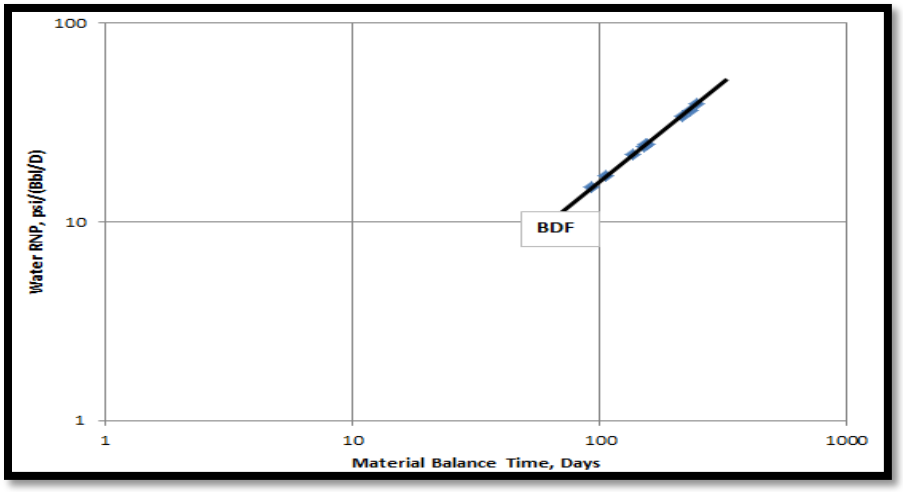

Fig.45. FF-5 reached BDF immediatly after the well was put in production.

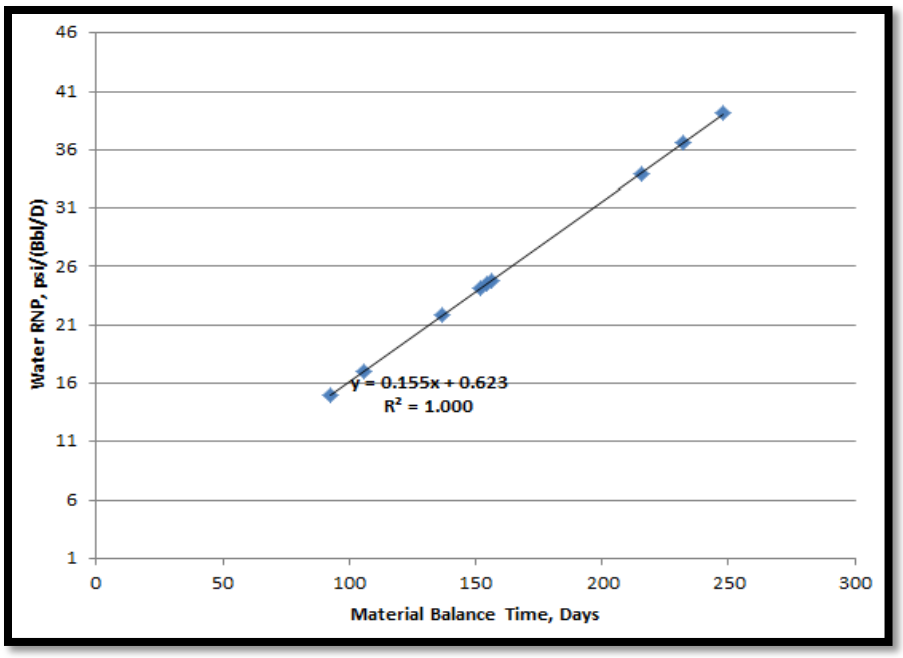

Fig. 46. m_{pss} for FF-5 is 0. 155 and it is obtained after 10 days of production.

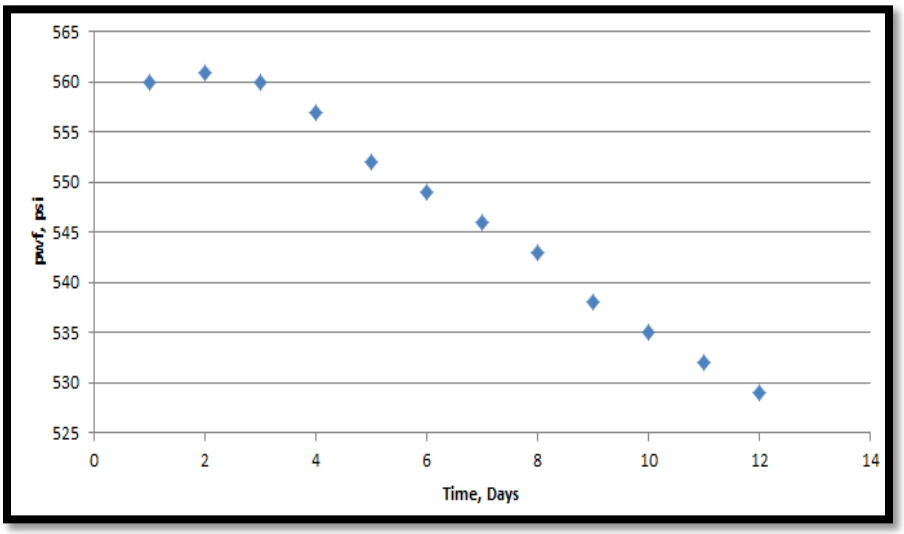

Fig. 47. The average flowing bottom-hole pressure for FF-5 is around 545 psi for the analyzed period (2-12 days).

Table 15 - Estimation of effective fracture volume for FF-5

Initial reservoir pressure	1,736 psi
Gas gravity	0.58
Reservoir temperature	118 ^{o}F
Cumulative injected water	58,093 Bbl
Cumulative produced water after around 3 years	9,167 Bbl
m_{pss}	0.155 $\frac{psi}{Bbl}$
Average flowing bottom-hole pressure in the analyzed period	545 psi
c_{gDD}(at 1191 psi)	9.030 * 10^{-4} psi^{-1}
C1 and C2 for Eq. 3.3	1.15 and 1.01
Calculated Water Volume	8,300 Bbl = 14.3 % of injected water

4.1.4 FF-6

Table 16 summarizes the results for FF-6. Fig 48, Fig.49, Fig. 50, Fig. 51 are used to perform our analysis and estimate the effective fracture volume

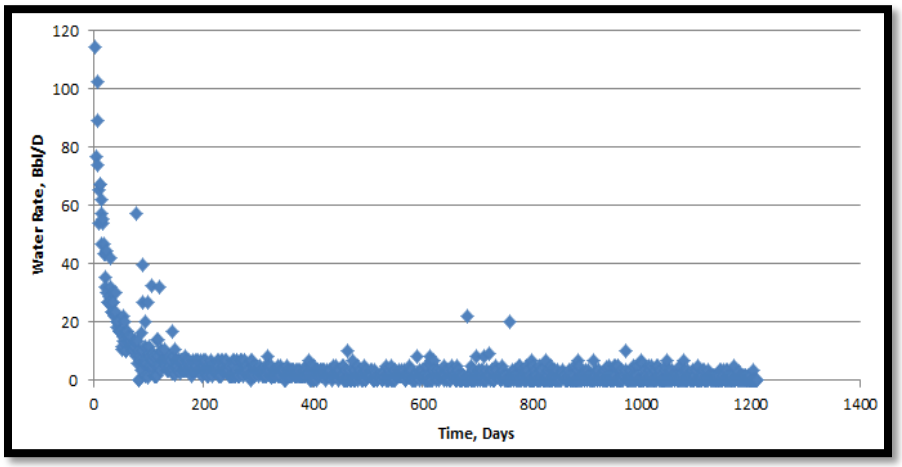

Fig 48. FF-6 Decline curve plot of water rate vs. time.

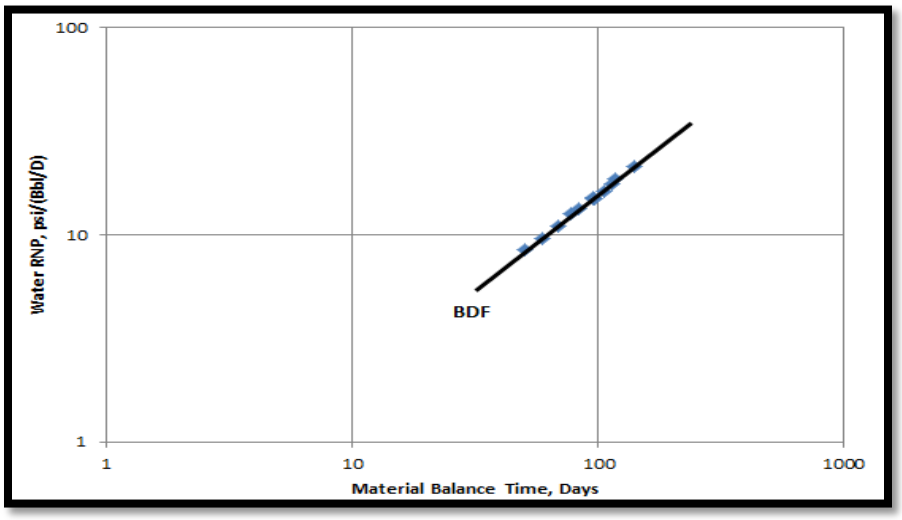

Fig.49. FF-6 reached BDF immediatly after the well was put in production.

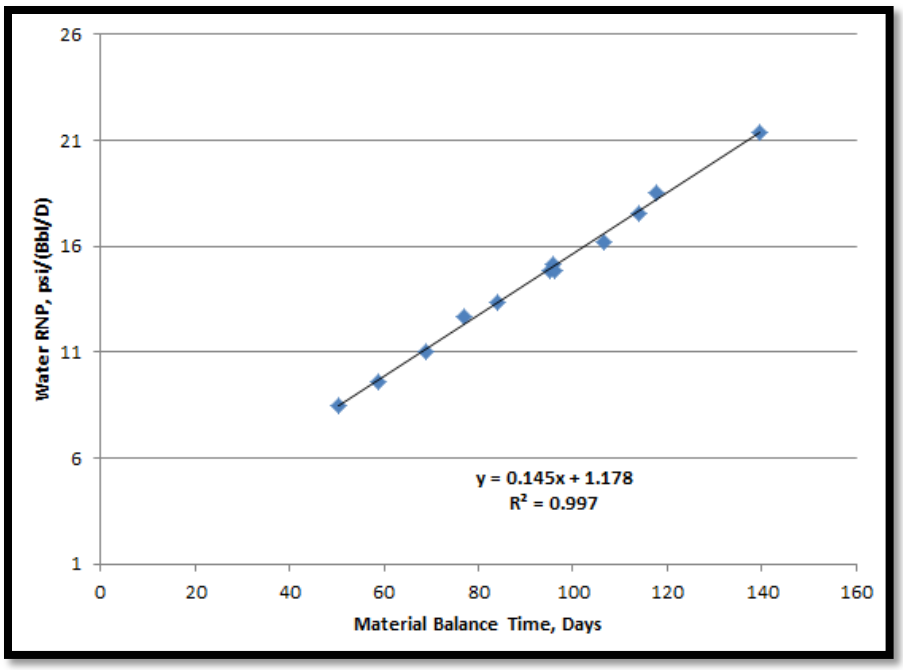

Fig. 50. m_{pss} for FF-6 is 0. 145 and it is obtained after 15 days of production.

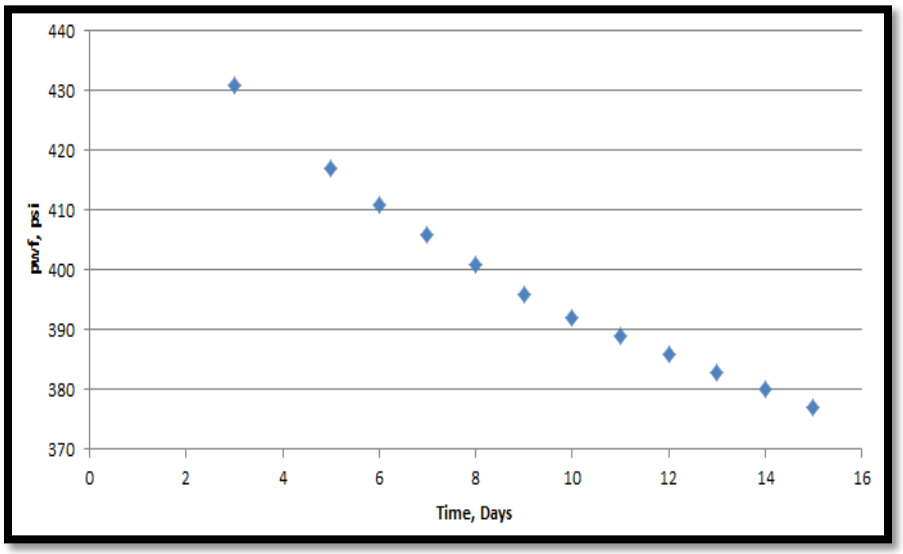

Fig. 51. The average flowing bottom-hole pressure for FF-6 is around 400 psi for the analyzed period (2-15 days).

Table 16 - Estimation of effective fracture volume for FF-6

Initial reservoir pressure	1,736 psi
Gas gravity	0.58
Reservoir temperature	118 ^{o}F
Cumulative injected water	68,914 Bbl
Cumulative produced water after around 3.3 years	10,839 Bbl
m_{pss}	0.145 $\frac{psi}{Bbl}$
Average flowing bottom-hole pressure in the analyzed period	400 psi
c_{gDD}(at 1336 psi)	8.057 * 10^{-4} psi^{-1}
C1 and C2 for Eq. 3.3	1.15 and 0.98
Calculated Water Volume	9,745 Bbl = 14.14 % of injected water

4.1.5 Discussion of Results

Using Eq. 3.3 gave an estimated effective fracture volume that represents 85%-90% of the total produced water when the water rate reached 1 Bbl/D or less. This difference can be caused by two reasons. First, it can be due to the fact that some water was produced from nearby fracturing job since the water rate showed unexpected increase in different periods during the well life. Second, this method does not work

perfectly in actual wells since the pressure used for the flowing bottom-hole pressure is actually estimated using the casing pressure.

The calculated volume ranged between 12-20% of the total injected volume. Although the method did not provide accurate estimations when field data were used, it still can be a good tool to evaluate the fracture jobs where it consistently underestimates all the wells by 10-15%.

CHAPTER V

CONCLUSION

The objective of this work was to test Alkouh's method in estimating effective fracture volume using water production data. Alkouh's method uses water rate normalized pressure (RNP), water material balance and gas compressibility in order to evaluate fracturing jobs.

Alkouh's method was based on the observation that gas flow affects the behavior of the water production data. Therefore, gas compressibility was used to analyze water production data. Alkouh's method assumes that the gas compressibility should be calculated at the initial reservoir conditions. Alkouh's method gave a much better estimate of the actual water volume comparing with the case when water compressibility and formation compressibility were used.

However, this study shows that Alkouh (2014) assumption of using gas compressibility at initial reservoir conditions is not valid. This was done by running several simulation cases with the same fracture volume and different initial reservoir conditions. It was concluded that reservoir temperature and gas gravity do not have significant effect on the calculations of the effective fracture volume (Cases 1A-1C and 2A-2C). However, the effect of initial reservoir pressure was significant where higher initial reservoir pressure values (lower gas compressibility) showed much larger volume estimates than lower initial reservoir pressure values (higher gas compressibility) since

we are dividing by gas compressibility to get the effective fracture volume (cases 3A-3D).

Finally, Alkouh's method did not consider the effect of the flowing bottom-hole pressure on the gas compressibility which also has a significant effect on the volume calculations as shown in cases 4A-4F. Therefore, it is suggested that gas compressibility should be evaluated at the drawdown pressure. In addition, two correlations (Fig. 25 and Fig. 34) are introduced so that the new method can give accurate estimation regardless of the initial reservoir pressure or the flowing bottom-hole pressure.

The new method was tested on the simulation cases and showed very good level of accuracy with an average difference of 3% only. Then, the new method was applied on four gas shale wells in Fayetteville reservoir using the first few days (10-15 days) after the well was put on production. It underestimated the effective fracture volume (produced water) by (10-15%). This difference should be acceptable since extra water might be produced as a result of nearby fracturing jobs.

REFERENCES

Abbasi, M., Dehghanpour, H., and Hawkes, R.V. 2012. Flowback Analysis for Fracture Characterization. Paper presented at the SPE Canadian Unconventional Resources Conference, Calgary, Alberta, Canada. Society of Petroleum Engineers SPE-162661-MS. DOI: 10.2118/162661-ms.

Alkouh, A.B. 2014. New Advances in Shale Gas Reservoir Analysis Using Water Flowback Data. Ph.D. Dissertation. Texas A&M University, College Station, Texas.

Alkouh, A.B., Wattenbarger, R. A., and Mcketta, S. F. 2013. Estimatoin of Fracture Volume Using Water Flowback and Production Data for Shale Gas Wells. Paper Presented at the SPE Annual Technical Conference and Exhibition, New Orleans, Louisiana, USA, 30 September–2 October 2013. doi:10.2118/166279-MS.

Chen, C.-C., Serra, K., Reynolds, A.C. et al. 1985. Pressure Transient Analysis Methods for Bounded Naturally Fractured Reservoirs. *SPE Journal* **25** (3): 451-464. doi: 10.2118/11243-pa

Clarkson, C.R. 2012. Modeling 2-Phase Flowback of Multi-Fractured Horizontal Wells Completed in Shale. Paper presented at the SPE Canadian Unconventional Resources Conference, Calgary, Alberta, Canada. Society of Petroleum Engineers SPE-162593-MS. DOI: 10.2118/162593-ms.

Clarkson, C.R. and Williams-Kovacs, J.D. 2013. A New Method for Modeling Multi-Phase Flowback of Multi-Fractured Horizontal Tight Oil Wells to Determine Hydraulic Fracture Properties. Society of Petroleum Engineers. doi: 10.2118/166214-MS.

De Swaan O., A. 1976. Analytic Solutions for Determining Naturally Fractured Reservoir Properties by Well Testing. *SPE Journal* **16** (3): 117-122. doi: 10.2118/5346-pa

El-Banbi, A., H. and Wattenbarger, R.A. 1998. Analysis of Linear Flow in Gas Well Production. Paper presented at the SPE Gas Technology Symposium, Calgary, Alberta, Canada. 1998 Copyright 1998, Society of Petroleum Engineers Inc. 00039972. doi: 10.2118/39972-ms

Kazemi, H. 1969. Pressure Transient Analysis of Naturally Fractured Reservoirs with Uniform Fracture Distribution. *SPE Journal* **9** (4): 451-462. doi: 10.2118/2156-a

Serra, K., Reynolds, A.C., and Raghavan, R. 1983. New Pressure Transient Analysis Methods for Naturally Fractured Reservoirs(Includes Associated Papers 12940 and 13014). *Journal of Petroleum Technology* **35** (12): 2271-2283. DOI: 10.2118/10780-pa

Warren, J.E. and Root, P.J. 1963. The Behavior of Naturally Fractured Reservoirs. *SPE Journal* **3** (3): 245-255. doi: 10.2118/426-pa

Williams-Kovacs, J.D. and Clarkson, C.R. 2013. Stochastic Modeling of Multi-Phase Flowback from Multi-Fractured Horizontal Tight Oil Wells. Paper presented at the SPE Canadian Unconventional Resources Conference, Calgary, Alberta, Canada, 5-7 November, 2013. doi:10.2118/166214-MS

APPENDIX A

GASPROP6

Input Data	
Sep. Gas Gravity (air = 1.0)	0.65
Oil/Gas Ratio, STB/MMscf	0
Oil Gravity, deg. API	55.8
H_2S,fraction	0
CO_2, fraction	0
N_2, fraction	0
Res. Gas Gravity (air = 1.0)	0.65
Res. Temperature, °F	160
Standard Temp, °F	60
Standard Pres., psia	14.65

Calculated Critical Values	
Tpc, R	356.72615
Tpr	1.7371028
Ppc, psia	668.57329

Single Pressure	
pressure (psia) =	3000
Results	
Z Factor =	0.8842
Bg (rcf/scf) =	0.005149
Bg (rbbl/Mscf) =	0.9169
c_g, (1/psi) =	3.011E-04
μ_g, (cp) =	0.0201
m(p), $(psi^2/cp)*10^{-6}$ =	607.9
density, (lb/ft^3) =	9.5998

Pressure	Correlated Properties						
(psia)	Z Factor	B_g (rcf/scf)	B_g (rb/Mscf)	c_g (1/psi)	μ_g (cp)	m(p) $(psi^2/cp)*10^{-6}$	density (lb/ft^3)
14.65	0.999	1.190836	212.0813	6.835E-02	0.0125	0	0.0415
100	0.991	0.17311	30.8299	1.009E-02	0.0126	0.7834	0.2855
200	0.982	0.08578	15.2769	5.089E-03	0.0127	3.188	0.5762
300	0.973	0.056681	10.0946	3.421E-03	0.0128	7.198	0.8720
400	0.965	0.042142	7.5052	2.586E-03	0.0129	12.81	1.1728
500	0.957	0.033426	5.9530	2.085E-03	0.0131	20.01	1.4786
600	0.949	0.027624	4.9196	1.749E-03	0.0132	28.78	1.7892
700	0.941	0.023486	4.1827	1.508E-03	0.0134	39.10	2.1045
800	0.934	0.020389	3.6312	1.327E-03	0.0136	50.95	2.4241
900	0.927	0.017987	3.2035	1.185E-03	0.0138	64.30	2.7478
1,000	0.920	0.016072	2.8624	1.070E-03	0.0140	79.12	3.0752
1,100	0.914	0.014511	2.5844	9.757E-04	0.0142	95.37	3.4060
1,200	0.908	0.013216	2.3537	8.958E-04	0.0144	113.0	3.7397
1,300	0.902	0.012126	2.1596	8.272E-04	0.0147	132.0	4.0759
1,400	0.897	0.011198	1.9942	7.675E-04	0.0149	152.3	4.4139
1,500	0.893	0.010398	1.8519	7.149E-04	0.0152	173.8	4.7532
1,600	0.889	0.009704	1.7282	6.679E-04	0.0155	196.5	5.0932
1,700	0.885	0.009097	1.6201	6.256E-04	0.0157	220.3	5.4333
1,800	0.882	0.008562	1.5248	5.873E-04	0.0160	245.3	5.7729
1,900	0.880	0.008088	1.4404	5.523E-04	0.0163	271.2	6.1112
2,000	0.878	0.007665	1.3652	5.202E-04	0.0166	298.1	6.4478
2,100	0.876	0.007288	1.2979	4.905E-04	0.0170	325.9	6.7818
2,200	0.875	0.006949	1.2375	4.631E-04	0.0173	354.6	7.1129
2,300	0.875	0.006643	1.1830	4.376E-04	0.0176	384.1	7.4405
2,400	0.875	0.006366	1.1337	4.139E-04	0.0180	414.2	7.7640
2,500	0.875	0.006115	1.0890	3.918E-04	0.0183	445.1	8.0831
2,600	0.876	0.005886	1.0482	3.712E-04	0.0187	476.6	8.3973
2,700	0.877	0.005677	1.0110	3.519E-04	0.0190	508.7	8.7063
2,800	0.879	0.005486	0.9770	3.338E-04	0.0194	541.3	9.0099
2,900	0.882	0.00531	0.9457	3.169E-04	0.0197	574.4	9.3078
3,000	0.884	0.005149	0.9169	3.011E-04	0.0201	607.9	9.5998
3,100	0.887	0.005	0.8904	2.863E-04	0.0205	641.8	9.8858

APPENDIX B

CMG CODE

```
RESULTS SIMULATOR IMEX 201210

INUNIT FIELD
WSRF WELL 1
WSRF GRID TIME
WSRF SECTOR TIME
OUTSRF WELL LAYER NONE
OUTSRF RES ALL
OUTSRF GRID SO SG SW PRES OILPOT BPP SSPRES WINFLUX
WPRN GRID 0
OUTPRN GRID NONE
OUTPRN RES NONE
**$  Distance units: ft
RESULTS XOFFSET         0.0000
RESULTS YOFFSET         0.0000
RESULTS ROTATION          0.0000  **$  (DEGREES)
RESULTS AXES-DIRECTIONS 1.0 -1.0 1.0
**$
        ************************************************************************
        **********
**$ Definition of fundamental cartesian grid
**$
        ************************************************************************
        **********
GRID VARI 27 27 1
KDIR DOWN
DI IVAR
 97.72904
 59.43149
 36.14179
 21.97874
 13.36582
 8.128095
 4.9429
 3.005902
 1.827965
 1.111632
 0.6760113
 0.4110995
 0.25
```

2
0.25
0.4110995
0.6760113
1.111632
1.827965
3.005902
4.9429
8.128095
13.36582
21.97874
36.14179
59.43149
97.72904

DJ JVAR

239.2871
135.053
76.2236
43.0204
24.28061
13.70391
7.734454
4.365306
2.463768
1.390544
0.7848197
0.4429502
0.25
2
0.25
0.4429502
0.7848197
1.390544
2.463768
4.365306
7.734454
13.70391
24.28061
43.0204
76.2236
135.053
239.2871

```
DK ALL
 729*300
DTOP
 729*7000

**$  0 = null block, 1 = active block

NULL CON           1


POR CON         0.06


PERMI CON      0.00015
MOD

14:14 1:27 1:1 = 1


PERMJ CON      0.00015
MOD

14:14 1:27 1:1 = 1

PERMK CON      0.00015
MOD

14:14 1:27 1:1 = 1



**$  0 = pinched block, 1 = active block
PINCHOUTARRAY CON           1
PRPOR 3000
CPOR 1e-6
MODEL GASWATER
TRES 160
**$        p       Eg       visg
PVTG EG 1

      14.696   4.73179  0.0125391
     213.716    70.303  0.0127104
     412.737   138.671  0.0129606
     611.757   209.809  0.0132688
```

```
     810.777   283.595   0.013631
      1009.8   359.784  0.0140459
     1208.82   437.991  0.0145132
     1407.84   517.683  0.0150317
     1606.86   598.192  0.0155993
     1805.88   678.756  0.0162121
      2004.9   758.585  0.0168651
     2203.92   836.928   0.017552
     2402.94   913.135  0.0182659
     2601.96   986.694  0.0189998
     2800.98   1057.24  0.0197469
        3000   1124.56  0.0205013

BWI 1.01412
CVW 0.0
CW 2.93601e-006
DENSITY WATER 61.9615
REFPW 3000
VWI 0.432871
GRAVITY GAS 0.65
ROCKFLUID
RPT 1
**$       Sw       krw
**$       Sw       krw
SWT
          0        0
          1     1
**$       Sg       krg
**$       Sg                 krg
SGT
          0                  0

          1                  1



INITIAL
USER_INPUT
PRES CON         3000
SW CON           0

*MOD
  14:14      1:27      1:1    = 1
```

```
NUMERICAL
DTMIN 1e-9
NORTH 40
ITERMAX 100
RUN
DATE 2000 1 1
DTWELL 1e-009

**$
WELL  'Well'
PRODUCER 'Well'
OPERATE  MIN  BHP  500.0  CONT
OPERATE  MAX  STG  1e+020  CONT
**$         rad  geofac  wfrac  skin
GEOMETRY  K  0.25  0.37  1.0  0.0
PERF  GEOA  'Well'
**$ UBA      ff   Status  Connection
   14 14 1  1.0  OPEN    FLOW-TO  'SURFACE'
LAYERXYZ  'Well'
**$ perf geometric data: UBA, block entry(x,y,z) block exit(x,y,z), length
   14  14  1    250.000485    550.000531    7000.000003    250.000485    550.000531
        7299.999997  300.000000
DATE 2000 2  1.00000
DATE 2000 3  1.00000
DATE 2000 4  1.00000
DATE 2000 5  1.00000
DATE 2000 6  1.00000
```